Microfluidic Analysis and Parallel Confocal Detection of Single Molecules

Michael Gösch

Karolinska Institute
Stockholm 2003

Microfluidic Analysis and Parallel Confocal Detection of Single Molecules

Doctoral Thesis
Institution of Medical Biophysics
Department of Medical Biophysics and Biochemistry
Karolinska Institutet
Stockholm
Sweden

ISBN 91-7349-663-4

“You can only find truth with logic if you have already found truth without it.”
Gilbert Keith Chesterton, *The Man Who was Orthodox*

Es gibt viele Theorien,
Die sich jedem Check entziehen,
Diese kann man aber checken,
Elend wird sie dann verrecken.
Christian Morgenstern

“Satisfaction lies in the effort, not in the attainment. Full effort is full victory.”
Indira Gandhi

To my family

Abstract

The detection of single molecules using confocal spectroscopy is of major interest and tremendous improvements have been made within the last decade. The underlying basics, however, a pinhole and a single excitation volume element have remained the same as well as the technical limitations. This thesis presents an approach to address and overcome these technological hurdles and to design and implement a confocal system with parallel detection capability that increases the throughput and speeds up the analysis time. Therefore, microfluidic systems, diffractive optical excitation, CMOS (Complementary metal oxide semiconductor)-detector arrays and the combination of these novel techniques have been investigated. In order to show the usefulness of these techniques, biomolecular applications like screening of Alzheimer's amyloid-β peptides and gene expression analysis have been investigated as well. In addition to that, microstructure systems together with confocal spectroscopy were used to degrade DNA on the single molecule level or to enrich biological samples.

Knowledge of flow behavior in microstructures is essential when microchannels are used for analytical applications. Fluorescence Correlation Spectroscopy (FCS) was utilized to investigate hydrodynamic pressure driven flow in microchannels with a cross section of 50 x 50 μm^2. The flow itself, was detected non-altered or non-invasively, since only tiny (a couple of nanometer in size) dye-molecules were entrained into the fluid. This was sufficient to determine the flow velocities in laminar layers of < 1 µm in size. Further, transport properties were monitored in microchannels with the help of a 1 x 4 diffractive optical element (DOE) induced laser excitation array.

A step forward towards a highly integrated parallel confocal fluorescent detection set-up has been taken, by introducing CMOS-detector arrays in conjunction with diffractive optical elements (DOEs). A combination of a 2 x 2 DOE and a 2 x 2 CMOS-detector array was utilized in order to see if parallel detection of single molecule is feasible. This detection scheme potentially improves and speeds up the analysis of biological and chemical samples because on-chip processing, data analysis, and a high level of integration could easily be realized.

Two individual DOEs were used to build a parallel 2 x 2 cross correlation set-up. This technology has been developed for the determination of the gene expression profile by a novel analytical method based on cross correlation analysis. Here, the long analysis time and the constantly present low concentration of the sample motivated the implementation of such a set-up. Additionally, other analytical methods such as high-throughput screening (HTS), could profit from this method decreasing their analysis time in future.

The detection of single molecules in flow has been illustrated and utilized, including investigations on single molecule detection in microchannels using elliptical shaped detection volume elements. With the present systems, Alzheimer's β–amyloid peptides were analyzed and a feasibility for up-concentration of biological or chemical samples was performed with regards to pl flow switching with external valves. Finally, DNA was degraded on the single molecule level and the cleavage rate of the enzyme was determined.

List of Papers

This thesis is based on the following papers, referred to in the text by their Roman numerals. The papers are reprinted by permission from the American Chemical Society, the Optical Society of America, the Institute of Electrical, and Electronics Engineers and Oxford University Press.

I **Michael Gösch**, Hans Blom, Johan Holm, Toni Heino, and Rudolf Rigler: "Hydrodynamic Flow Profiling in Microchannel Structures by Single Molecule Fluorescence Correlation Spectroscopy", *Analytical Chemistry*, **72**, 3260-3265 (2000) © American Chemical Society.

II Hans Blom, Mathias Johansson, **Michael Gösch**, Toni Sigmundsson, Johan Holm, Sverker Hård, and Rudolf Rigler: "Parallel flow measurements in microstructures by use of a multifocal 4 x1 diffractive optical fan-out element", *Applied Optics*, **41** (31), 6614 – 6620 (2002) © Optical Society of America.

III **Michael Gösch**, Alexandre Serov, Alexis Rochas, Hans Blom, Tiemo Anhut, Pierre-André Besse, Radivoje S. Popovic, Theo Lasser and Rudolf Rigler: "Parallel Single Molecule Detection with a fully integrated Single Photon 2x2 CMOS Detector Array", submitted to *Journal of Biomedical Optics.*

IV Alexis Rochas, **Michael Gösch**, Alexandre Serov, Piere-André Besse, Radivoje S. Popovic, Theo Lasser and Rudolf Rigler: "First Fully Integrated 2D-Array of Single Photon Detectors in Standard CMOS Technology", *IEEE Photonics Technology Letters*, **15** (7), 963-965 (2003) © Institute of Electrical and Electronics Engineers.

V Kerstin Korn, Paola Gardellin, Bohao Liao, Mario Amacker, Åsa Bergström, Henrik Björkman, Agnès Camacho, Sabine Dörhöfer, Klaus Dörre, Johanna Enström, Thomas Ericson, Tatiana Favez, **Michael Gösch**, Adrian Honegger, Sandra Jaccoud, Markus Lapczyna, Erik Litborn, Per Thyberg, Holger Winter and Rudol Rigler: "Gene Expression Analysis using Single Molecule Detection", *Nucleic Acid Research,* **31**, 16, e89 (2003) © Oxford University Press.

VI **Michael Gösch**, Hans Blom, Per Thyberg, Anders Magnusson, Sylvain Anderegg, Sverker Hård, Theo Lasser and Rudolf Rigler: " Multi-focal dual-color cross-correlation spectroscopy of single biomolecules using diffractive-optical-elements", submitted to *Optics Letters.*

VII Hans Blom, Niklas Bark, **Michael Gösch**, Per Henriksson, Toni Sigmundsson, Gunnar Björk and Rudolf Rigler: "Analysis of Amyloid β-peptides in fluidic microchannels", Manuscript.

VIII **Michael Gösch**, Thomas Ericson, Bohao Liao, Stefan Wennmalm, Mario Amacker, Anders Hanning, Jenny Hellström, Tore Niklasson, Sabine Dörhöfer, Åsa Bergström, Christian Vieider, Claes Ek and Rudolf Rigler: "Towards DNA sequencing on the Single Molecule Level with laser trapped beads in hydrodynamic flow", Manuscript.

Acknowledgements

Thanks to all who have contributed to this thesis with, for instance, simply a smile at the right time and place, to cheer me up when I needed it the most. However, some people have contributed with more than that and therefore I would like to Thank in particular;

Rudolf Rigler for his unlimited support and enthusiasm, for all the freedom I was given, for finding a solution (always), for all the friendly chats in between, and for the trust he put in me.

Theo Lasser for his support and friendship. For introducing me into his group and letting me participate in many decision processes.

Hans Blom for fun in the lab, his support and for his unbreakable commitments.

Thomas Ericson for teaching me Svenska språket, showing me the nice Ångermanlandet and Swedish lifestyle. For being a good friend and showing me around in his life and Stockholm.

Kerstin Korn for the (conspirative) chats in between and for extra lessons in Biology.

Holger Winter for letting me participate in his pleasure and pain, for his Senator card and for his feedback for written scientific articles as well as this thesis.

Erik Litborn for having been a wonderful roommate. Do I have to explain more…?

Lars Edman for believing, featuring and supporting me in any possible way.

Stefan Wennmalm for accompanying me all the years and patience when it comes to my Swedish.

Per Thyberg for his natural way of explaining complicated mathematical relations.

Niklas Bark for showing an interest in physics and for his longing for perfection.

Sylvain Anderegg and **Per Henriksson** for being my diploma students.

The people at GNOTHIS for their interest and encouragement with regards to my research and for accompanying me on my journey towards my thesis and giving a helping hand whenever I needed it.

Jerker Widengren for following my education with interest and for scientific advice.

Per Rigler for his engagement in the lab, all the meetings we had and the chats and fun in and outside the EPFL.

Alexandre Serov for being a positive and caring person and his dry Russian humor.

Alexis Rochas for explaining the CMOS detector to me (even though I still do not get it) and for everything related to it and **Pierre-André Besse** for proof-reading my paper in the most detailed way, for concrete feedback and his patience.

Mona Wells for being the only person ever, reading this thesis twice, and for giving me all the nice little comments, which helped me a lot and cheered me up during the last phase of my thesis.

Lars Kappei for food, joy and happiness, for the heavy leisure time program I had to attend and for always being in a good mood.

Ivo Willrodt for being in touch with me, for fun and ages of friendship.

Alexander Friedrichs, who helped me to survive my first year in Sweden and for being the friend I saw far to seldom.

Claes Ek for his leadership, experience and trust in my abilities.

Christian Vieider for being a great boss, for still working together with me even though he already knows me quite well, and for his fantastic meals on his boat.

Gunilla Edeborg for every single advice, for giving me comfort in any situation and food in the evening. Simply for listening and caring!

Karl-Anton Büning for always showing his interest in the “painted” molecules I had to look at.

Knut Radbruch for helping me with math when I needed it most and for following my education with interest.

My **sister** for always letting me feel that she is proud of me.

My **mum** and **dad**, where would I be today without you?

My **grandma** for her view of the world.

My **grandpa** who was the first to show me the beauty of math and physics and who somehow still tries to make me understand German grammar.

My brother **Flo** who helped me to think a little bit further and to defocus from myself.

And finally, **Frauke**, for all the encouragement, trust, patience and comfort you gave me in the last couple of years.

I reserve the Right to **Thank** anyone else whom I may have inadvertently forgotten.

Stockholm
October 2003 *Michael Gösch*

Table of Contents

Glossary

µTAS	Micro total analysis system
APD	Avalanche photo diode
Aβ–peptide	Amyloid β-peptide
Bp	Base pair
CCD	Charge-coupled device
CDNA	Complementary DNA
CMOS	Complementary metal oxide semiconductor
cw	Continuous wave
dCTP	2'-deoxycytosin 5'-triphosphate
DNA	Deoxyribonucleic acid
DNAbp	DNA-binding protein A variant
DOE	Diffractive Optical Element
DRIE	deep reactive ion etching
dsDNA	Double stranded DNA
dUTP	2'-deoxyuridine 5'-triphosphate
EL-1	Human transcription elongation factor 1-α 1
FCCS	Fluorescence Cross-Correlation Spectroscopy
FCS	Fluorescence Correlation Spectroscopy
FRET	Fluorescence Resonance Energy Transfer
FTV	Flow-tagging velocimetry
HTS	High-through screening
IR	Infra red
LIF	Laser induced fluorescence
MTV	Molecular tagging velocimetry
Nd:YAG	Neodymium:yttrium-aluminium-garnet
Nt	Nucleotide
P65	human transcription factor NF-κB p65 subunit
PAF	Photo activated fluorophore
PCR	Polymerase chain reaction
pFCCS	Parallel Fluorescence Cross-Correlation Spectroscopy
PGK1	mRNA encoding phosphoglycerate kinase
PIV	Particle image velocimetry
PMMA	Polymethylmetacrylate
PMT	Photo multiplier tube
RAB1	Human GTP-binding protein
RhGreen	Rhodamine green
RT-PCR	Real time PCR
S19	human s19 ribosomal protein
S/N	Signal to noise
SEM	scanning electron microscopy
SMD	Single molecule detection
SPAD	Single photon avalanche diode
SPCM	Single photon counting module
ssDNA	single stranded DNA
TMR	Tetramethylrhodamine
TP	target principle
tuba	human tubulin alpha
UV	Ultra violet
VHS	(very) high speed dispensing valve

Symbols and Notation

τ_{diff}	Diffusion time
τ_{flow}	Flow time
Δp	Pressure difference
η	Viscosity
Δh	Height difference
ν	Count rate per molecule
ω_g , ω_r	Radial half-axis of green, red detection volume element
ω_{xy}	Radial half-axis of detection volume element
ω_z	Axial half-axis of detection volume element
C	Concentration
C_t	Fluorescence threshold value
d	Half-width of channel
f	Focal length
$G(\tau)$	Autocorrelation function
$G_r(\tau), G_g(\tau)$	Autocorrelation of the red channel, green channel
$G_{gr}(\tau)$	Cross-correlation
Hz	Hertz
I	Intensity
I_g, I_r	Intensity in green channel, red channel
k_R	Recombination rate of molecules in a given detection volume element
l	Length of channel
L	Lens
N	Number of molecules in sample volume
N_g, N_r	Number of molecules labeled with green dyes, red dyes
N_{gr}	Number of molecules labeled with red and green dyes
Q_R^R	Relative fluorescent detection efficiency (red excitation/red emission)
Q_B^R	Relative fluorescent detection efficiency (blue excitation/red emission)
Q_R^G	Relative fluorescent detection efficiency (red excitation/green emission)
Q_B^R	Relative fluorescent detection efficiency (blue excitation/red emission)
R	Ratio of axial to radial half-axis of detection volume element
R_C	Radius of the sphere-like laser focus volume element
S/N	Signal-to-noise
T	Measurement time
V	Size of detection volume element
var	Variance
V_{flow}	Flow velocity
V_{gr}	Cross-correlation detection volume element
x	Number of sample volumes
z_g	Axial half-axis of green detection volume element
z_r	Axial half-axis of red detection volume element

1. Introduction

The detection of single molecules in solutions can be performed by confocal fluorescence spectroscopy.[1-19] Here, researchers such as Keller, Rigler, Zare, Moerner, Trautman and their coworkers laid the foundations for single molecule research in solutions. The advantage of this technique lies in the high signal-to-noise (*S/N*) ratio that can easily be achieved in natural biological environment at room temperature. As analytical methods, fluorescence correlation spectroscopy (FCS)[20,21] and photon burst analysis[22-25] are commonly used. However, detecting single molecules of interest (having a size of a few nanometers) in 'large' sample volumes (in the µl-range) is as difficult as searching for a needle in a haystack. The goal of this thesis was to design, develop and test a novel single molecule confocal detection set-up with a higher integration level, focused on parallel and high throughput detection concepts, without jeopardizing specificity, accuracy, and sensitivity and with the goal of decreasing analysis time. For this reason, different tools and technologies, like microfluidics,[26] diffractive optical elements (DOEs)[27,28] and complementary metal oxide semiconductor (CMOS)[29]-detector arrays were investigated and later combined for biomolecule analysis. Biological applications like Gene-expression analysis, the screening of Alzheimer's Amyloid-β peptides, and DNA degradation studies with the aim to sequence DNA (deoxyribonucleic acid) the single molecule level have been performed in order to show the need and applicability of these technical advances.

Microfluidic devices have become more and more popular in the academic as well as the industrial world.[30-35] The main objectives in implementing microfluidic devices are; less reagents, lower costs, faster analysis, higher sample throughput and the possibility to achieve higher integration and automation. Here, a whole branch of analytical chemistry has been formed also referred to as micro-total analysis systems (µTAS). In such small devices, flow can be induced without undue difficulties. However, the knowledge of flow behavior in microfluidic structures and the methodology for monitoring flow in microfluidic channels are limited. Therefore, FCS has been used as a non-invasive and non-disrupting measurement tool to investigate flow properties with micrometer resolution in microfluidic structures (paper I). With this method, it was ascertained, that for analytical flow velocities, laminar flow was present microfluidic channels. At the same time a simple but novel tool to monitor the flow in microfluidic channels was developed. This might be of importance for micro-analysis and -probing devices where flow has to be ascertained and controlled at any instant of time. As an extended feature, DOEs were introduced into the laser beam

path and parallel flow monitoring was performed (paper II). With the DOE, four different excitation spots (detection volume elements) were generated and positioned in the microchannel to monitor flow at four different positions, simultaneously. Finally, the same set-up was used to study transport properties and the influence of diffusion onto pressure driven liquid transport of single molecules between two points in a microchannel.

Single molecule detection at low concentrations, for slow diffusing molecules, or for many samples with certain characteristics can become difficult, time consuming, or even impossible with FCS when single spot excitation and detection is applied.[36,37] Therefore, the number of detection spots was increased by using a well-mastered industrial CMOS process and fabricating a 2 x 2 integrated so-called CMOS-SPAD (Single Photon Array Detector) working in the Geiger mode.[29,38-41] This 2 x 2 CMOS-SPAD array combined with 2 x 2 DOE generated excitation volume elements was investigated for integrated parallel fluorescence single molecule detection feasibility and compared to a state-of-the art single-photon counting module (SPCM) actively quenched avalanche photo diode (APD) by making a series of measurements on freely diffusing molecules at different concentrations (paper III). In addition to the 2 x 2 CMOS detector array for parallel single molecule detection, a 32 pixel array has been developed and tested for parallel detector performance attributes like cross-talk, afterpulsing and dark count rate, results from which show that such a detector array allows for an even higher integration level (paper IV).

Dual-color cross correlation analysis (FCCS)[42-48] has widely been used in order to analyze and detect biomolecules in low concentration samples with a significantly higher selectivity, specificity, and accuracy that can be achieved with FCS. Utilizing this method, the expression level of genes in cells, which can differ by three orders of magnitude in the pM-regime, has been determined with dual-color cross-correlation analysis (paper V). Due to the high selectivity of the dual-color cross correlation analysis method, no amplification step like PCR (polymerase chain reaction) is needed and an unique and novel tool for drug validation and drug development was established. For this analysis, two dye-labeled DNA probes were hybridised to a selected gene target and using FCCS the absolute number of dual-labeled fragments was determined. Given this number, the number of target molecules within the biological sample was calculated in copies/µg cDNA using a calibration curve, which was generated with gene specific DNA beforehand. As this method is extremely sensitive there are some limitations with respect to high throughput analysis and analysis

time. Therefore, a parallel dual-color cross-correlation set-up was built and experiments on dual-color labeled samples were performed (paper VI). Again, parallel detection and analysis on a simple but effective integration level was used to decrease the measurement time and to broaden the scope for other potential applications. Here, two individually designed DOEs were inserted into the red and green laser beam paths generating four dual-color cross-correlating spots, and the performance of the multiple spot configuration was then tested by FCCS with different artificially dual-labeled cross-correlating PCR generated samples.

In addition, after determining that the flow in microfluidic structures was stable and controllable (paper I), microfluidic channels were used to screen for molecules of interest (paper VII). A statistically relevant result for diffusing Alzheimer's Amyloid beta (Aβ)-peptides could not be obtained, since the peptide size was too big and the concentration too low. Therefore, in order to increase the number of events and to make the quantification of Alzheimer Aβ-peptides more feasible the peptides were loaded into microchannels and a pressure driven sample stream was utilized to let the peptides flow through a cylindrical detection volume element, where they were detected. In addition to that, attempt undertaken to select molecules of interest from, for instance, chemical and biological libraries by applying external valves to microfluidic structures is presented as well.

DNA sequencing on the single molecule level was first proposed by Keller and coworkers in 1989.[1,49] In the last decades, endeavors in this subject area have resulted in numerous publications.[50-58] The latest progress has been reported by Werner *et al*.[59] Based on these results, investigations to achieve repeatable DNA degradation in a flowing enzyme stream in microstructures were made (paper VIII). Special emphasis was given to the so-called target principle (TP), upon which parameters like the size of the detection volume element, the distance between the DNA loaded bead and the detection focus, the flow velocity and the transport properties of the nucleotides were elaborated. Procedures for the alignment of the bead with respect to the detection volume element as well as some results of this intensified research will be summarized. Again this research is focused on high throughput DNA sequencing with the ultimate goal to be able to sequence, for instance, whole genes, which with contemporary sequencing machines is not possible.

The thesis concludes with a summary and outlook on the future work.

2. Flow Analysis in Microchannels (papers I & II)

Microfluidic devices are in popular use in both industry and academia. Potential benefits of such microfluidic devices in comparison to macroscopic devices are small sample volumes, improved accuracy and specificity, disposability, and user friendliness. However, the number of devices that utilize the full advantage of a miniaturized system is only slowly growing. The final goal for every researcher or developer in this field is the 'lab-on-a-chip' system.[26,60,61] Here, multiple technologies from modern biology, chemistry and medicine are combined into a single entity. In particular, applications and probing technologies like DNA analysis (e.g. PCR),[31,62] enzyme analysis (for example acetylcholinesterase[32] analysis), cytometry,[63,64] cellular biosensors and cell culturing[65,66] can be performed in microfluidic systems. Depending on the application, electroosmotic[67-72] or pressure driven flow[73-76] is applied to control sample transport in microchannels. Often, multiple channels with junctions and crossings are used to control and manipulate the sample. Since the analyte might be detected or mixed in a certain region of the microfluidic system laminar flow is required. Despite elaborate flow simulations prior to fabricating new microstructures, the user often has to test if the experimentally obtained flow is in accord with the theoretically predicted values. In addition, a permanent and simple flow-controlling unit can be desirable for commercial products or microfluidic systems running for a considerable time. For these purposes various flow monitoring techniques such as optical Doppler tomography,[77-81] particle image velocimetry (PIV)[30,82] and NMR imaging[83] can be used. However, some methods have to introduce particles into the flowing liquid, which can potentially induce flow disturbance. In order to avoid introducing particles that can disturb the flow during the measurement process new measurement techniques such as molecular tagging velocimetry (MTV)[84] and flow-tagging velocimetry (FTV)[85,86] were introduced. Unfortunately, these methods exhibit a purely spatial resolution because they have to be performed over large-length scales due to the long excited-state lifetime (tens of microseconds) of phosphorescent dyes, there length scales being equal to the distance the molecules have to travel in the microchannel from the point were they are excited ('tagged') to the point were their fluorescence is detected. In addition, the phosphorescent dyes very often require far ultraviolet (308 nm) excitation, which limits the window materials through which these measurements can be made. As an alternative to phosphorescent dyes, caged dye techniques utilizing one laser to 'un-cage' a photo activated fluorophore (PAF)[85] and a second to interrogate

the resultant fluorescent dye can be used. Thereby, even extremely fast flows (47 m/s) can be monitored.[35]

A high spatial resolution and a short measurement time can be achieved with FCS. Here, a diffraction limited excitation laser beam, which produces a spot that (depending on the wavelength) is below 1 µm in size, determines the resolution for the measurements of the laminar layer and thus flow can be investigated and monitored with sub-micrometer resolution. Fluorescent dye molecules in sub-nanomolar concentrations are mixed into the flowing liquid to determine the flow velocity. Molecules passing the excitation volume element are excited and the subsequent radiation from fluorescent relaxation is directly collected and directed to an APD. The APD translates the incoming photons into TTL pulses, which are routed to a computer where an autocorrelation curve is computed from which the flow velocity is determined.

2.1. FCS for Flow Profiling - Theory

The idea of FCS is based on observing the intensity fluctuation of fluorescence from individual molecules in a small open volume element defined by a laser beam with a Gaussian intensity profile. In the early 70s, Elson[87] and Magde[88,89] as well as Ehrenberg and Rigler[90] derived the principle theory behind FCS. In the following 30 years the basic formalism has been extended or changed depending on the application.

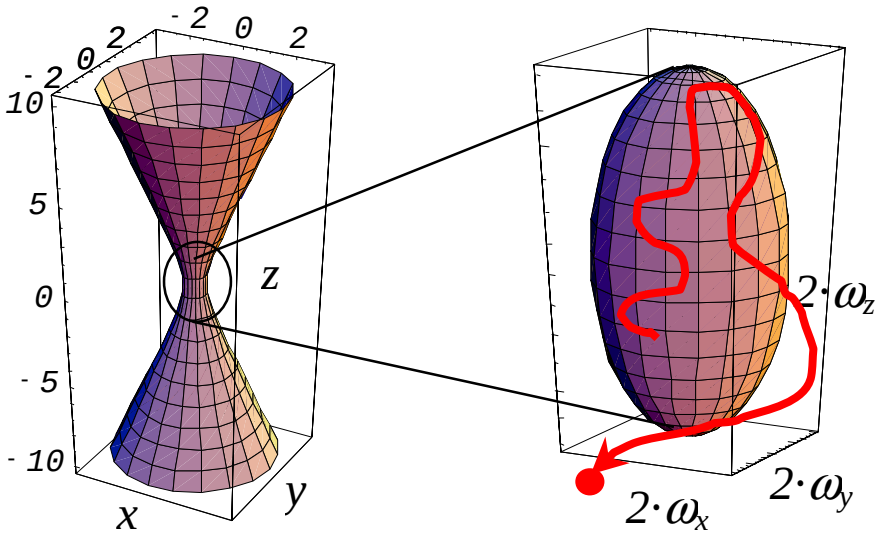

Figure 1 (left) Gaussian laser excitation profile. (right) Confocal volume of observation. The dimension of the observation volume element is defined by the half-axis in length (ω_z) and width (ω_{xy}). The ratio $R = \omega_z / \omega_{xy}$ between the two axes is often around 5 and ω_{xy} is typically just below 1 µm.

To understand FCS, lets assume we have a small confocal volume of observation, which happens to be filled with laser light (Figure 1). This laser light excites molecules and subsequent fluorescence is recorded and displayed as intensity I. Since the spatial coordinates of molecules in solution fluctuate due to Brownian motion, the intensity will fluctuate, too. Looking at an intensity trace, the fluctuation in time, δI, will be distributed around the mean intensity $\langle I \rangle$. This information already is sufficient to say something about the movement of the molecules and the number of molecules in the volume. We assume that molecules approach the observation volume by Brownian motion. A molecule entering the excitation volume element emits photons, and depending on the random walk of the molecule, it may remain a while, emitting some more photons, maybe even crossing the whole detection volume element, or alternately, it may quickly exit the volume element having emitted only a single photon to the detector. This randomized behavior can be recorded in the form of a correlation function of the measured intensity fluctuations of the molecules. The typical shape of an autocorrelation has a high amplitude for shorter timer ranges (100 ns – 1 ms) and almost no amplitude for longer time ranges (> 1 ms). The decay from the highest to the lowest point of the autocorrelation is exponential, logarithmic, or depending on the application and shape of the excitation volume element, a combination of these. Therefore, the highest ordinate value of the autocorrelation curve accounts for the fact that every molecule occupies the excitation volume element for at least a short time, whereby only a few molecules stay for a long time in the detection volume element, generating lower ordinate values. The overall amplitude of the autocorrelation function is inversely proportional to the average number of molecules in the detection volume element and its half-width gives the average cross-sectioned diffusion time of the molecules. With this information, the size of the excitation volume element can be calculated and thereby, the concentration and flow velocity of molecules obtained.

After this qualitative description of the autocorrelation curve, now the autocorrelation function will be derived in a more formalized way. The commonly used normalized autocorrelation function, which relates the fluorescence intensity, $I(t)$, at a time, t, to that τ seconds later, $I(t+\tau)$, is

$$G(\tau) = 1 + \frac{\langle \delta I(0) \delta I(\tau) \rangle}{\langle I \rangle^2}. \qquad (1)$$

In order to use this equation for the evaluation of experimentally obtained autocorrelation functions, the following analytical expression has been derived:[88,91,92]

$$G(\tau) = 1 + \frac{1}{\mathbf{N}}\left(1 + \frac{\tau}{\tau_{diff}}\right)^{-1}\left(1 + \frac{\tau}{R^2 \cdot \tau_{diff}}\right)^{-1/2}. \qquad (2)$$

Here, **N** is the average number of molecules in the observed volume element, τ_{diff} is the time that the molecules need on average to cross the observation volume element in the radial direction, which is equal to the average occupation probability of the molecules in the observation volume. The ratio of the axial to radial half-axis of the observation volume is R, where $R = \omega_{xy} / \omega_z$. The analytical expression for flow can be derived as follows:[89]

$$G(\tau) = 1 + \frac{1}{\mathbf{N}} \cdot A \cdot \exp\left\{-\left(\frac{\tau}{\tau_{flow}}\right)^2 \cdot A\right\}, \qquad (3)$$

where

$$A = \left(1 + \frac{\tau}{\tau_{diff}}\right)^{-1}\left(1 + \frac{\tau}{R^2 \cdot \tau_{diff}}\right)^{-1/2} \qquad (4)$$

and τ_{flow} is the average flow time of the molecule through the observation volume in the radial direction. Equation 3 reduces to equation 2 for $\tau_{flow} \to \infty$, which corresponds to a flow velocity of $V = 0$. Fitting equation 3 to the experimentally obtained autocorrelation curve gives the value for τ_{flow}. In order to determine the detected flow velocity, V_{flow}, the following equation should be used[89]

$$V_{flow} = \frac{\omega_{xy}}{\tau_{flow}}, \qquad (5)$$

$\omega_{xy} = \sqrt{4D\tau_{diff}}$ and D is the diffusion coefficient of the fluorescing molecules in the sample.

In addition to the FCS theory, the laws of hydrodynamic pressure also have to be considered. The relationship between the pressure difference, Δp, from the bottom to the top of a column of liquid having a height, h, is $\Delta p = \rho g h$, where ρ is the liquid's density and g is the gravitation constant. The applied pressure difference over a liquid-filled microchannel results in a stationary flow with the velocity V_{flow}. Since the liquid velocity is zero at the lateral faces and highest in the middle of the channel, a hyperbolic flow profile inside the channel is established, which can be expressed by the Hagen-Poiseuille-equation:

$$V(x) = \frac{\Delta p}{2\eta l}\left(d^2 - x^2\right) \qquad (6)$$

where η denotes the liquid's viscosity, l the length, d the half width of the microchannel and x the coordinate in the channel.

2.2. Microchannels and Set-up – Experimental

All microstructures used in this experiment were fabricated by ACREO AB, Kista, Sweden, using standard micro-machining technologies, which included thin film deposition, photolithography, etching and wafer bonding. Deep reactive ion etching (DRIE) was applied to etch microchannels with flat lateral faces and cross sections up to 50 x 50 µm^2 into the silicon wafer. Finally, the channels were covered by a glass wafer, which was thinned down to 170 µm to match the optical properties for a water immersion objective. In Figure 2 SEM images of a typical microstructure are displayed.

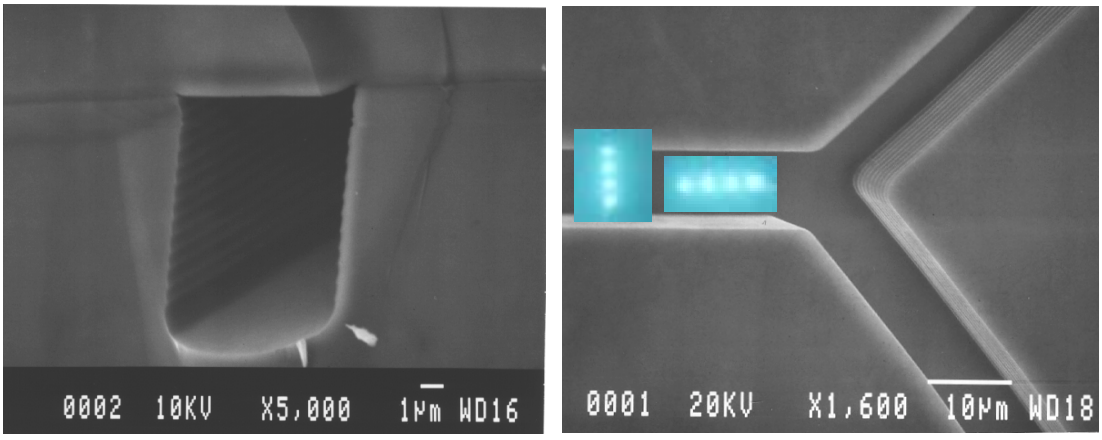

Figure 2 (left) Cross-section of a 10 x 10 µm^2 microchannel. (right) SEM picture of a 10 x 10 µm^2 etched microchannel. In addition, the fluorescence pattern from the 4 x 1 diffractive optical fan-out element is displayed (for more details see text). The foci are numbered in the text 1, 2, 3 and 4 from top to bottom in the pattern on the left and from left to right in the pattern on the right.

The experimental detection set-up consisted out of an argon laser (515 nm), focused into the microchannel by a 60x water immersion objective. Molecules (TMR-4-dUTP), passing the focus were excited and resulting fluorescent light was collected through a confocal pinhole, recorded by an APD and translated into an autocorrelation curve. Equation 3 was fitted to the obtained curves with a self-made program (Corrkino, KI), where the maximum likelihood estimates of the parameter for equation 3 were obtained by non-linear optimization according to Marquardt.[93] Finally, the flow velocity, V, was calculated from the resulting flow-diffusion time, τ_{flow}, with equation 5.

2.3. Flow Profiling in Microchannels - Results

In the first experiment, the laser focus was positioned in the middle of the channel, where, due to the hydrodynamic flow profile (equation 6), the highest flow velocity was detected. Changing the height of the reservoir increased the pressure difference, Δp, and thereby the flow velocity, V. For higher flow velocities, the exponential term of the autocorrelation function for uniform flow (equation 3) became more pronounced, which led to a steeper curve (see Figure 3, left). Consequently, τ_{flow} became smaller, too.

In the second experiment, the reservoir was raised in consecutive steps and for every position the autocorrelation curve was recorded. As predicted by equation 6 a linear dependency between Δp ($\propto$ reservoir height, h) and the flow velocity V was obtained for measurements consistently performed at a single spatial coordinate, x (see Figure 3, right).

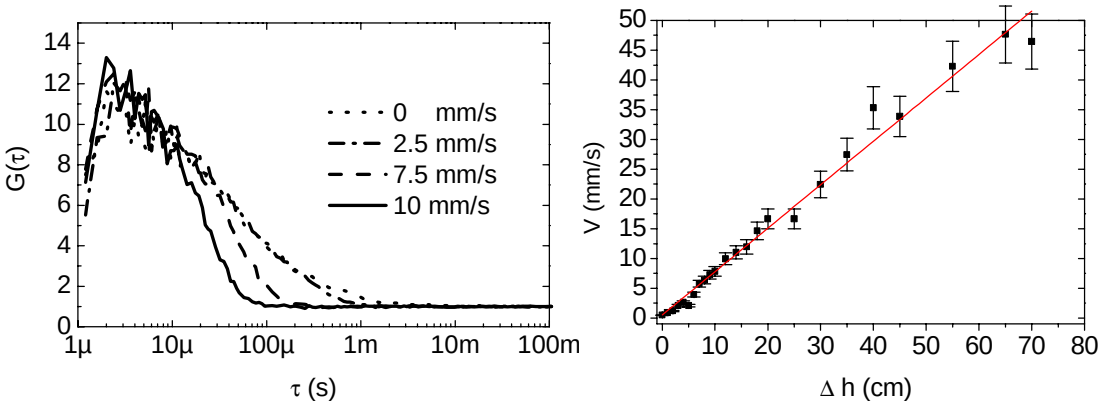

Figure 3 (left) Autocorrelation curves for different flow velocities in the middle of the microchannel. (right) Flow velocity in the middle of the channel in relation to the height difference between the inlet and the outlet of the fluidic system.

Additionally, flow profiling with sub-µm precision was performed. Here, a 50 µm x 50 µm^2 small channel was scanned from the top to the bottom and from the left to the right in µm-steps with a detection volume element having ω_{xy} = 0.4 µm detection volume element (the size of the detection volume element was determined beforehand with free diffusing TMR-4-dUTP). The results show a clear hydrodynamic flow profile in microchannels, which follows the law of Hagen-Poiseuille (see Figure 4 and equation 6). Deviations in the maximum flow velocities can be explained by a slight miss-positioning in height of the confocal spot in the channel. The experiments illustrated that, even in the micro-sized world, hydrodynamic laws are valid and laminar instead of turbulent flow is obtained. In addition, a non-invasive tool for flow monitoring in micro-sized fluidic structures was developed.

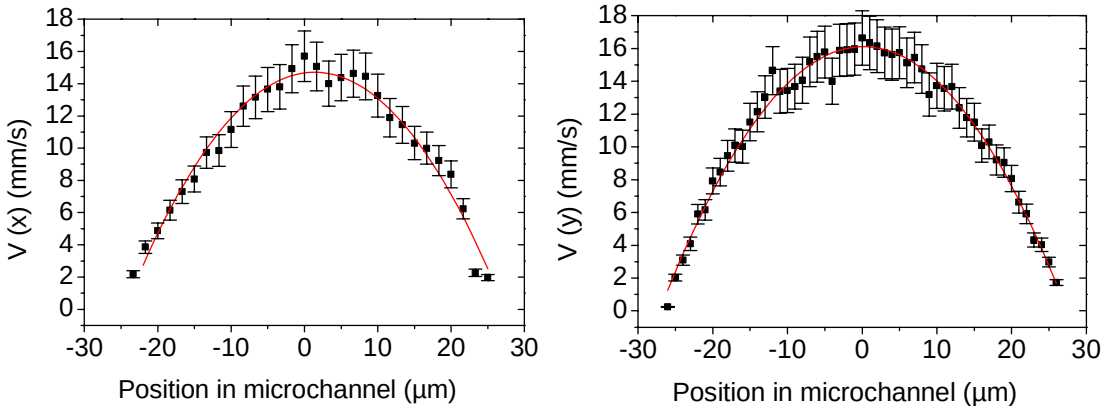

Figure 4 Flow profiled in the microchannel scanned in the horizontal (left) and vertical (right) directions. These velocities have been determined at a reservoir height of 20 cm (*V*= 15 mm/s).

2.4. Parallel Flow Analysis and Transport Properties of Dye-labeled Nucleotides in Microchannels – Results

The same laminar flow profile in microstructures has been detected in a parallel manner with the help of a 4 x 1 DOE[27] (for details on DOEs see[28,94]) excitation. Here, the incoming laser beam passed a 4 x 1 fan-out DOE, which manipulates the light through phase modulation and results in a diffractive redistribution of the laser intensity, in this case a 4 x 1 foci pattern. The first diffraction order generates four foci with almost equal intensities (variations between the foci were less than 4 %). Fluorescence emission was collected by four individual fiber coupled APDs. Almost 80 % of the overall laser intensity entering the DOE was found for the four spots. The other 20 % are found in the higher order refraction spots. The foci spacing was a = 2.78 µm under the 60 x water immersion objective and all the foci could easily be

positioned in a 20 x 20 µm^2 microchannel either parallel or perpendicular to the flow (see Figure 2, right). To measure the flow velocities at four different spots simultaneously, solutions with dye-labeled nucleotides (nts) where injected into microchannels and the four foci were first positioned perpendicular to the microchannel flow. The autocorrelation was recorded for each of the four foci, simultaneously. The autocorrelation curves for each focus were analyzed for different reservoir heights and the values for τ_{flow} determined. With help of equation 5, the flow velocity was calculated and displayed for each spot and at different reservoir heights (Figure 5, left).

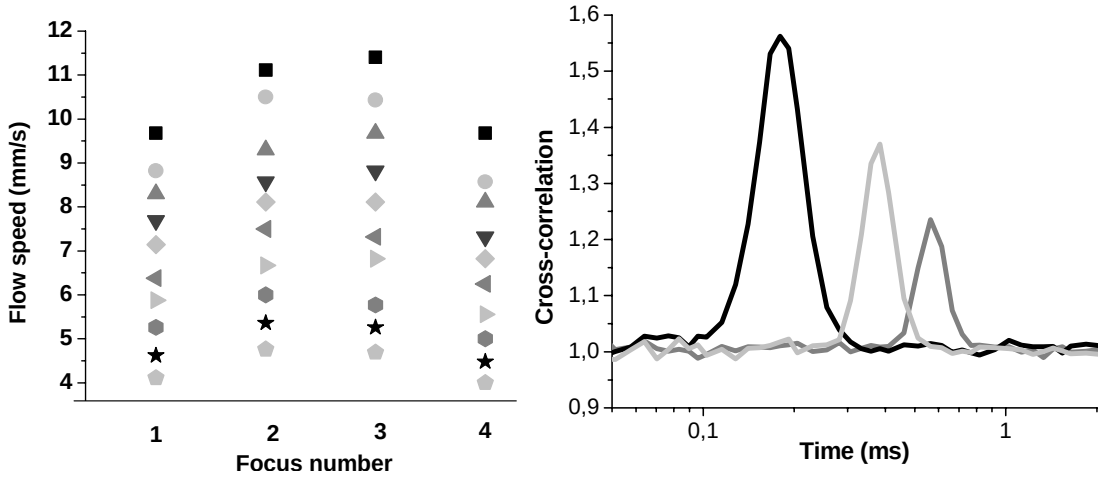

Figure 5 (left) Parallel flow profiling at different reservoir heights between 85 cm (top) and 40 cm (bottom) inside the 20 µm microchannel. (right) . Cross-correlated flows at a reservoir height of 90 cm. Focus 1 and 2 (black), focus 1 and 3 (light grey), and focus 1 and 4 (grey).

Finally, the signal of the first DOE generated spot was cross-correlated[95] with the other three spots (Figure 5, right). Thereby, a probability distribution of the recovered molecules, transported by the laminar flow over a certain distance, was determined. For these measurements, the four spots were positioned in the middle of the channel in direction of the flow (see Figure 2, right). Here, the cross-correlation amplitude ratio is a direct measure of the percentage of molecules that passed both the first and the next spot. Comparing the cross-correlation result from the spots 1-2 with the result from the spots 1-3 and 1-4, a decrease in amplitude is seen. If the cross correlation amplitude would result in the same amplitude from spot 1-2 and 1-3 for example, all molecules would have been detected in the second spot as well. However, due to Brownian motion, the molecules experience a lateral displacement, which makes it impossible to recover all molecules passing the first detection volume element in the next spot. Dividing the second amplitude (0.375) with the first amplitude (0.575) gives the fraction of molecules that originate from one spot and pass to a consecutive de-

tection spot. The result is that 65 % of the molecules could be found at the distance a = 2.78 µm downstream originating from one spot for a flow velocity of approximately 15 mm/s. Consequently, only 40 % of the molecules originating from the first spot were found after a distance of 2 a = 5.56 µm.

2.5. Conclusions – Flow Analysis in Microchannels

First, a non-intrusive convenient technique, which allows the determination of flow velocities in laminar layers at increments of < 1 µm in two dimensions has been presented. Properties which are important for any flow-dependent analytical method in microchannels can be monitored with this method.

Second, the flow velocities in a microstructure can be changed in a controlled way with a simple hydrodynamic pressure set-up. However, since this set-up requires long silicon tubes (at least as long as h), syringe pumps (Univentor 864) have been used for later applications. These pumps automatically control the pressure on the syringe pistons and thereby the flow velocity in the microchannel. Different syringe sizes allow for varying the volumetric flow from 0.001 µl/min up to 5 ml/min. Also, calibration curves (not shown), where the velocity in the channel is measured as a function of the volumetric flow, were established and afterwards the same type of calibration technique was used in other experiments like DNA degradation and Aβ-peptide screening in flow (vide infra). The confirmation that laminar flow was present in µm sized flow channels enables the analysis and manipulation of liquid samples, and applications such as single molecule DNA sequencing and single molecule detection (SMD), screening and fractioning can be performed in microfluidic structures with a well designed flow scheme.

Finally, a parallel flow analysis system that allows for simultaneous monitoring of different laminar layers in microstructures was presented. With this method, independent measurements of different flow velocities in for instance capillaries for DNA sequencing or other microfluidic multichannel devices become feasible. Additionally, a method studying transport properties over a lateral distance of less than 10 µm was established, whereby the transport effects on diffusion as a function of distance can be studied. This method can also be used to increase the detection probability or to improve the determination accuracy of molecules passing through a multiple foci array down stream. Thereby, the detection of molecules at low concentrations as well as molecules exhibiting low count rates could be improved.

3. Parallel FCS and Single Molecule Detection with CMOS-Detector Arrays (papers III & IV)

Laser induced fluorescence (LIF) applications require excitation, wherein the whole sample is illuminated or a single confocal laser focus is scanned across the sample. High-throughput sequence analysis for gene expression, drug target validation and identification with DNA microarrays are superb examples of applications,[96-98] where the number of excitation spots can range from a few to several thousand.[99] In order for these techniques work, a huge number of fluorescence molecules are needed to produce a sufficiently high signal. Often, the microarrays are completely illuminated with one light source resulting in non-optimized power usage and undesired scattering. Instead, the confocal spectroscopy based ultra-sensitive analytical method presented above can be implemented. Altering this method from single spot excitation to multiple excitation spot arrays produced with the help of DOEs, parallel detection concepts with an efficient power usage can be established without sacrificing ultra-high sensitivity and high spatial resolution. Blom *et al*. performed the first measurements on dye molecules utilizing a 2 x 2 fan-out DOE,[100] thereby transforming the commonly used single excitation spot into four spots with equal intensity and with Gaussian laser excitation profiles. The number of spots that can be generated with this method is basically unlimited and only dependent on the total excitation intensity that is available.

In order to have a fully functioning parallel fluorescence-based analytical system for biomolecules, detection modules with multiple active areas have to be implemented in conjunction with multiple excitation spots. Here, most of the microarray analytical systems utilize CCD-based detection systems,[101] where the sensitivity for these systems is good, but the resolution is restricted by the pixel size of the CCD detector (5-20 µm). In addition, the long read-out time makes fast real-time dynamical studies in the range from 1 ns to 1 ms impossible. Therefore, detectors and transducers capable of single photon detection are required for single molecule analysis[38] and time resolved spectroscopy or time-gated detection schemes require detectors with sub-ns single photon timing jitter.[102,103] FCS measurements are mostly performed with detectors such as solid state SPCM or even photomultiplier tubes (PMTs)[104] which have low dark count rates, large detection areas and a relatively high detection probability. The SPCM is especially suited because of its robustness, long operating lifetime, good timing resolution, the high detection probability over a wide spectral

range, insensitivity to magnetic fields, and simple TTL pulse output, the latter of which is compatible with most of the commercially available photon counting modules. However, detection systems utilizing multiple excitation foci (see chapter 2) need one PMT or one SPCM for each spot. Ramping up the system to multiple spots consequently raises the price of the detection module enormously and requires sophisticated solutions for the alignment of the set-up. More over, state of the art SPCMs[105] cannot be implemented in an array, because the product is based on a non-CMOS compatible process where the readout electronics cannot be integrated on the same chip.

A well-mastered industrial CMOS process has been used to fabricate a 2 x 2 integrated CMOS-SPAD array working in the Geiger mode, which allows for multiple simultaneous single molecule analysis. With this 2 x 2 CMOS-SPAD detector array the emission from multiple 2 x 2 DOE foci excited molecules was detected. In particular the performance of the single-photon CMOS detector was investigated and compared to a state-of-the art SPCM (having an actively quenched APD), by using both to make measurements on freely diffusing molecules at different concentrations. Finally, the potential of this technique for high throughput FCS based detection systems will be discussed.

3.1. CMOS-SPAD Array Performance, Set-up – Experimental

3.1.1. Design

The CMOS-SPAD consists of a fully integrated 2 x 2 array (OUT 1 – OUT 4 in Figure 6) implemented with an active quenching circuit. The detector works in the Geiger mode, which means that a single photon can initiate avalanche breakdown. The pitch between the pixels is 1100 µm and which corresponds (with demagnification) to the distance between the spots of the 2 x 2 DOE generated pattern in the sample (the same DOE has also been used a the publication by Blom *et al*.[100]). A schematic of the active area of the SPAD and of a single CMOS-SPAD with integrated electronics is shown in Figure 6 a) and b). The pulse amplitude was 1.4 V and therefore sufficient to be used as an input pulse for the Flex990EM-12 digital correlator (www.correlator.com) and to record autocorrelation curves.

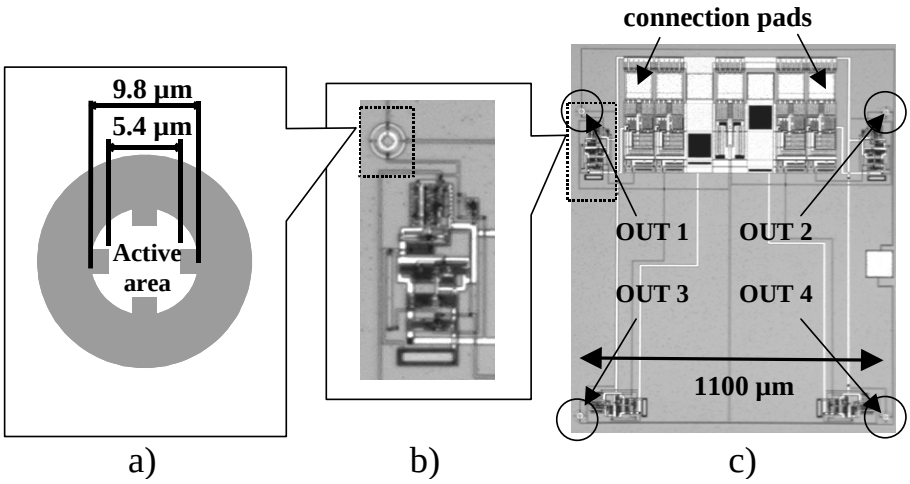

Figure 6 a) Geometrical configuration of a single CMOS-SPAD. The effective diameter of the sensitive area corresponds to 7-8 µm; b) single CMOS SPAD with integrated electronics; c) chip of 2 x 2 CMOS-SPAD array. OUT 1 – OUT 4 show the positions of the active areas. The distance between the photodetectors (active areas) is 1100 µm.

3.1.2. Dark Count Rate

The dark count rate was dependent on different excess bias voltages (see Figure 7, left). An acceptable excess bias voltage had to be found for room temperature in order to make the detector as sensitive as possible, but at the same time to keep the dark count rate low. An excess bias voltage of V_e = - 2.5 V was found to be appropriate for the measurements. With this excess bias voltage the dark count rate of the four detectors in the 2 x 2 SPAD array were 40, 30, 400, and 2000 Hz for OUT1 to OUT4, respectively. Obviously, the fourth detector suffers from fabrication imperfections. However, in a later generation detector array with 32 detectors, which has been produced in a completely new and obviously cleaner fabrication line of the silicon foundry, the dark counts were significantly reduced. In this 32 detector array, all but five pixels (four of those having a dark count rate < 150 Hz) exhibited a low dark count rate of about 50 Hz at room temperature. Only one pixel had a dark count rate of about 3800 Hz. Cooling the system to –20 °C reduced this detector's high dark count rate a hundred fold to about 300 Hz and all other detectors had a dark count rate of below 10 Hz.

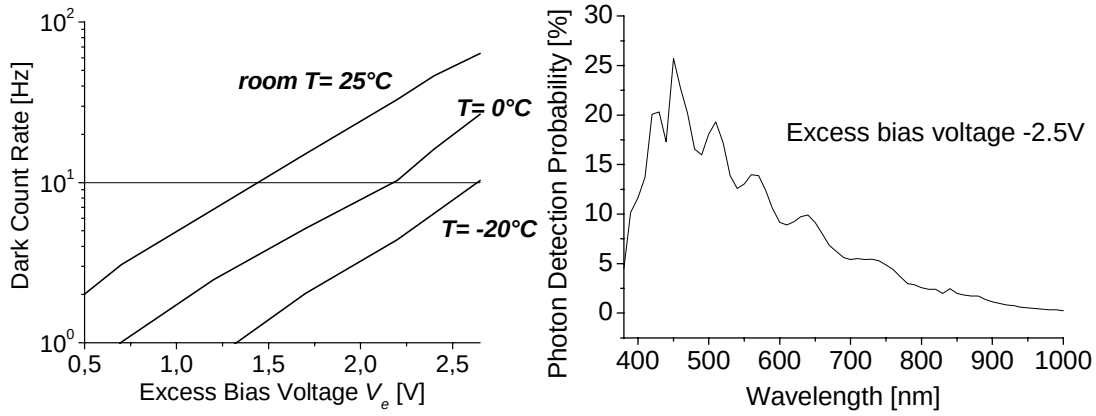

Figure 7[¥] (left) The dark count rate is highly dependent on the temperature and the excess bias voltage. For room temperature a reasonable dark count rate (< 250 Hz) was obtained for an excess bias voltage of V_e = -2.5 *V*. (right) Photon detection probability of the detector in use. The detector is most sensitive in the blue and green regions (450 – 550 nm). Working in the area of 550 nm, the photon detection probability was between 10 % and 15 %.

3.1.3. Photon Detection Probability

One of the most important features of single photon detectors is the photon detection probability (see Figure 7, right), because it can significantly decrease the analysis time for various applications. For the CMOS-SPAD detector array a photon detection probability of 5 – 15 % was attained in the region 500 – 700 nm. This is a factor of five to ten lower than for commercially available SPCMs. In addition, the detector is poorly optimized for wavelengths around 700 nm, in which many commercial available dyes (e.g. Cy5) are fluorescent. The photon detection probability determines the experimentally obtained count rate per molecule, ν. For **N** >> 1 and for molecules with a low ν, which is the case for molecules detected with the CMOS-SPAD, the relation[36,37,106]

$$S/N = \frac{G(\tau)}{\sqrt{\mathrm{var}(G(\tau))}} \approx \nu\sqrt{T}\,, \qquad (7)$$

is valid, which means that a $\nu_{\text{CMOS-SPAD}}$ being 5 to 10 times smaller than $\nu_{\text{SPCM-APD}}$ would entail a 25 to 100-fold increase in measurement time for the former to achieve the same S/N as the latter. However, for concentrations with **N** << 1, equation 7 changes and becomes $S/N \sim \sqrt{\mathbf{N}}$.[36,107] Then, for a set-up with multipoint excitation and detection, the registered number of fluorescent molecules, **N**, increases linearly

[¥]Figure 7 is reproduced with the kind permission of A. Rochas.

with the number of observation volume elements, x, and with regards to equation 7 the signal-to-noise ratio will increase with the square-root of it; $S/N \sim \sqrt{x \cdot \mathbf{N}}$. Here, the autocorrelation curves for each detector should of course be analyzed separately in order to keep the background low. Since the fabrication process of the CMOS-SPAD is not fully developed yet, it can still be modified towards increased photon detection probabilities. Thereby, even single spot detection with a CMOS-technology SPAD, would be superior to the SPCM detector, because of its higher integration level and its possibility for on chip processing of the collected data.

3.1.4. Afterpulsing

Another important benefit of the CMOS fabrication process is the complete disappearance of afterpulsing, which results from the release of carriers trapped in the multiplication region during an avalanche process. If such a release happens after the recharge of the SPAD, the trapped carrier induces an unwanted pulse, which is correlated with the previous avalanche event. Currently, these effects are simply neglected or not taken into account for FCS measurements. This is not a severe effect for the determination of diffusion times of molecules under observation. However, estimation of the number of molecules and their triplet lifetimes will be biased by the afterpulsing effect, which gives a severe contribution in the time range of $\tau < 1$ ms.[21] In Figure 8, a normalized autocorrelation curve for white light source illumination (10 kHz) of a CMOS SPAD is displayed along with that of a commercially available SPCM-AQR-13 (Perkin Elmer Optoelectronics).

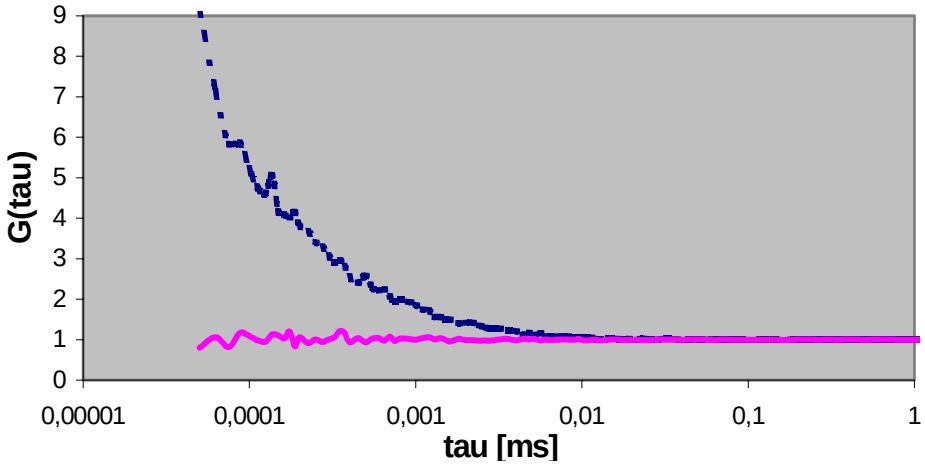

Figure 8 Autocorrelation curves of the CMOS SPAD (grey) and the SPCM-AQR-13 (dark and dashed) given white light source illumination at 10 kHz.

3.1.5. Set-up

The set-up, which has been used for the measurements described in the next section, is displayed in Figure 9. The laser beam from a diode pumped solid-state laser (532 nm, Kimmon, model-5526) was enlarged by a beam expander (L_1 (f = 25 mm), L_2 (f = 400 mm)) to fully illuminate the DOE and to overfill the back aperture of the microscope objective. With the use of collimators (L_3 (f = 150 mm), L_4 (f = 150 mm)) the microscope objective and a dichroic mirror in conjunction with the DOE, the expanded beam was shaped into a 2 x 2 foci pattern and focused into the sample. The collimated DOE spots were reflected by a dichroic mirror (Chroma, 565LP) into a 40x NA 1.15 water immersion objective (Olympus, Uapo/340, cover slip corrected) and the intensity in a single spot was measured to be 1.7 mW at the back aperture of the objective. Fluorescence emission from the sample was collected by the same objective and passed by the same dichroic mirror through a band-pass filter (Chroma HQ585/40) that filtered Rayleigh and Raman scattered light. Finally, the fluorescence emission was focused by a tube lens (L_5 (f = 180 mm)) and a four times de-magnifying lens (L_6 (f = 35 mm)) onto either one detector (∅ 7-8 µm) of the 2 x 2 CMOS SPAD array (see Figure 6) or onto an optical fiber (∅ 9 µm) connected to the SPCM-AQR-13. The set-up for single–point measurement was realized without the DOE in the beam path.

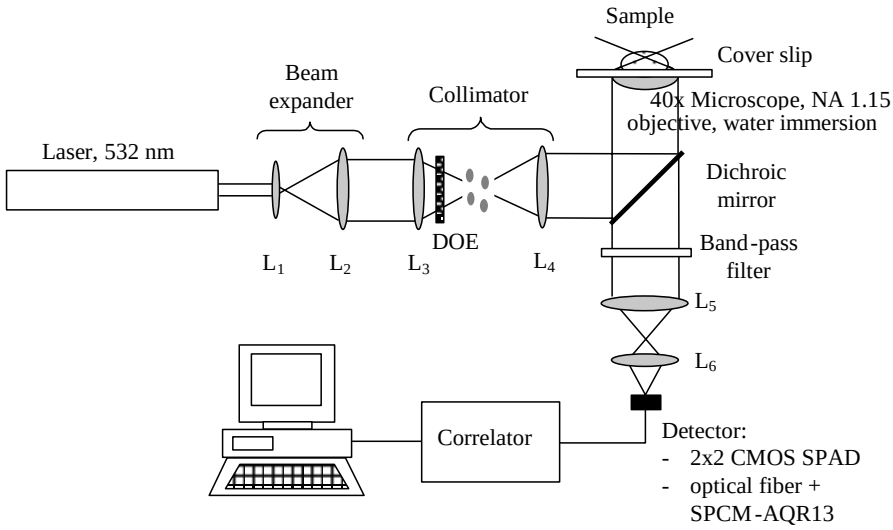

Figure 9 Experimental set-up for parallel FCS measurements.

3.2. Comparison CMOS-SPAD vs. SPCM-APD – Results

3.2.1. Influence of the Measurement Time on Statistical Reliability

FCS measurements were performed with both the CMOS-SPAD and the SPCM-APD detector on TMR molecules (500 pM) to determine the influence of the measurement time on statistical reliability. The measurements are displayed in Figure 10 and show the measured number of molecules in the detection volume element and the diffusion time as functions of the acquisition time (averaging time) chosen to be 1, 3, 5, 7, 10, 15, 20, 30, 45, and 60 seconds, respectively. The dependence of the fitting error on the acquisition time is shown on the right ordinate for each graph.

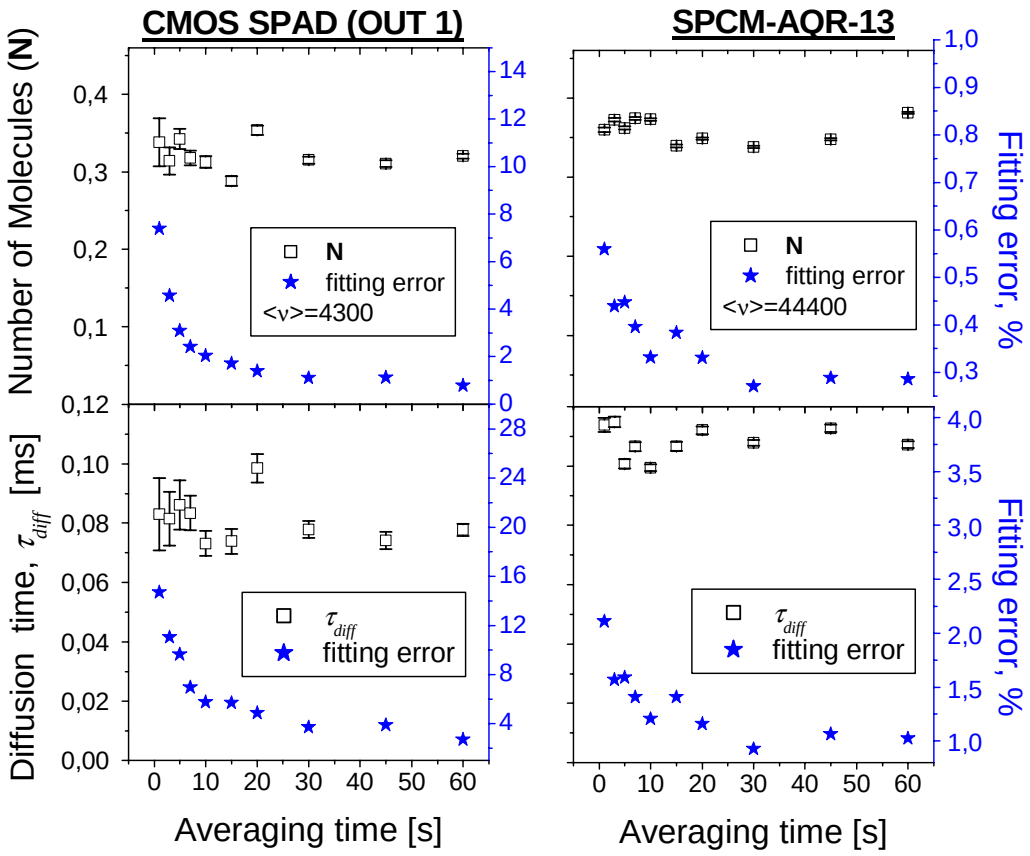

Figure 10 Left ordinate-axes: measured number of molecules (**N**) in the sampling volume and diffusion time (τ_{diff}) as functions of the averaging time. Right ordinate-axes: fitting error. Measurements were done with the CMOS-SPAD (left column) and a commercial single photon counting module (SPCM-AQR-13, right column) on TMR nucleotide molecules at 500 pM concentration. ν represents the experimentally observed count rate per molecule.

The average number of fluorescent molecules from which the concentration ($C \propto \mathbf{N}$) can be determined, and the diffusion time (τ_{diff}) were obtained by fitting the measured

correlation curve with the analytical autocorrelation function described above (see equation 2). The number of photons detected within a certain time interval influenced the 'smoothness' of the correlation function, and thus decreased the standard deviations in τ_{diff} and **N**, which in turn finally influenced the precision of the estimated values of τ_{diff} and **N**. Therefore, the experimental obtained data from the SPCM-AQR-13 (Figure 10, right) had a smaller fitting error and consequently a better measurement statistics, where overall the estimates of **N** and τ_{diff} are precise to within 0.6 % and 2.5 %, respectively ($p < 0.05$). The maximum fitting errors obtained with the CMOS-SPAD (Figure 10, left) were precise to within 8 % and 16 %. However, for longer averaging times the fitting error was strongly reduced, and even in the sub-single molecule measurement regime (**N** < 1) the CMOS detector a good statistical precision with fitting errors smaller than 1.2 % for **N** and smaller than 5 % for τ_{diff} for an acquisition time of 20 seconds. The different statistical precision that we obtained with the two detectors can be explained by the S/N for FCS measurements (see equation 7). The CMOS-SPAD fitting error is approximately ten times higher than the fitting error of the SPCM-APD due to lower ν obtained. This shows how important a higher detection probability would be for the CMOS technology produced detector to become a competitive product compared to the SPCM-APD, and certainly the CMOS-SPAD detection probability should be improved in the future. However, we would also like to point out that the measurements performed with the CMOS-SPAD at 500 pM TMR concentrations already yielded good results precise to within 5 % after only 5 seconds for the determination of **N** and after 15 seconds for the determination of τ_{diff}.

3.2.2. Multi-focal Detection with CMOS-SPAD

The 2 x 2 CMOS-SPAD array was used together with the multi-focal DOE-FCS system to demonstrate its feasibility for parallel FCS experiments. Solutions of 5 nM and 1 nM TMR (Figure 11, left and right) were dispersed in a droplet onto a cover glass. Then, the 2 x 2 fan-out DOE foci were positioned into the droplet. The count traces, obtained from the TMR solution, show the real-time fluctuations of the fluorescence signal (right columns). The average count rate for all four detectors was in the same range, which means that the sensitivity of all four detectors was almost identical. The autocorrelation functions, measured over 300 seconds by four different CMOS-SPADs, were similar but not identical (left columns). The reason for this is first, due to differences between the individual detectors (different dark count rates, vide supra)

and second, due to a slight positioning inaccuracy of the conjugated confocal spots on the detectors. For the 5 nM solution, the first three detectors gave us an average value of <**N**> = 3.5 ± 0.7 (standard deviation), $\langle \tau_{diff} \rangle$ = 96 ± 10 µs and ν = 2880 ± 500 Hz. The last detector gave higher value for **N** (= 6) and τ_{diff} (= 124 µs) and a value for ν (= 1235 Hz) that was lowered by a factor of almost three even when background noise was taken into account.[4,108] However, the calculated values of the TMR concentration obtained with all four detectors were quite similar (3.6, 4.4, 4.5, 4.8 nM). Concentration values were calculated with the following assumptions: the diffusion coefficient[92] was estimated to be 2.6x10^{-10} m^2/s and the formula for the volume of observation was: $V = R \cdot (4\pi\tau_{diff} D)^{3/2}$.

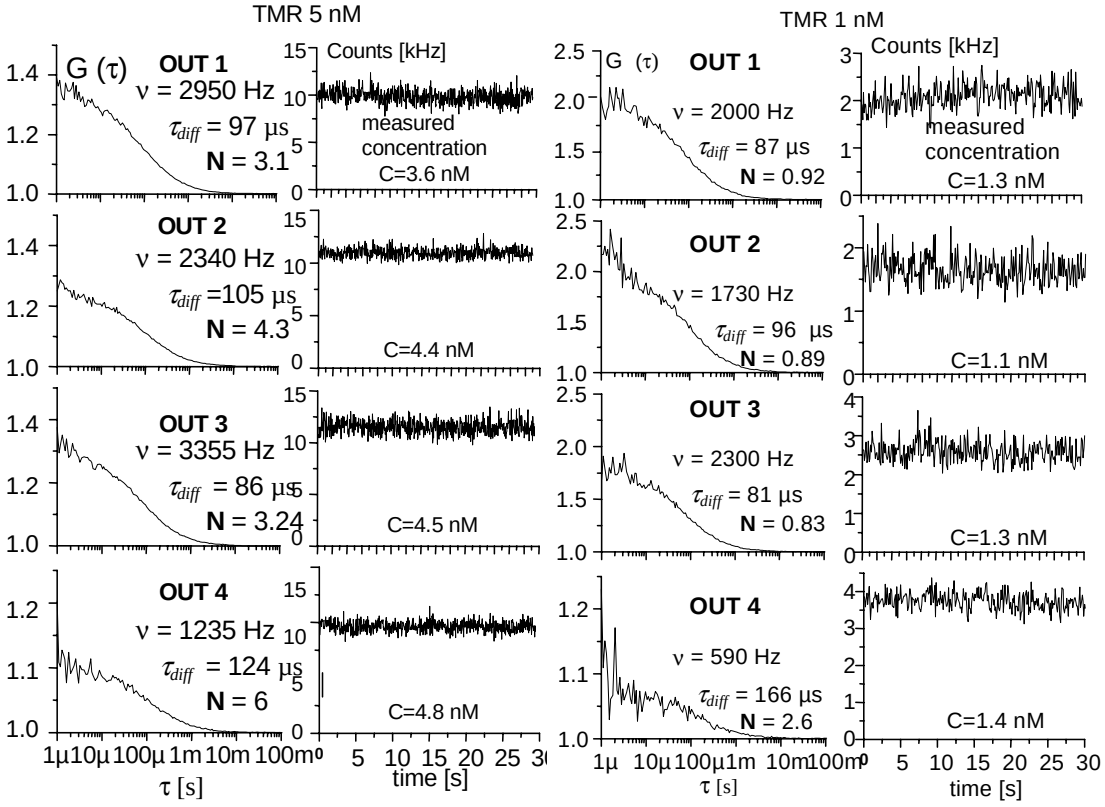

Figure 11 Autocorrelation functions (left columns) of fluorescent signals (right columns) measured with a 2 x 2 CMOS-SPAD from four DOE generated foci in 5 nM (left panel) and 1 nM (right panel) suspensions of TMR dye molecules, ν represents the experimental observed count rate per molecule.

The 1 nM TMR concentration was measured with the 2 x 2 FCS system to demonstrate parallel detection capability on the sub-single molecule level (**N** < 1). Here, the first three detectors gave us an average number of molecules <**N**> = 0.88 ± 0.04, an

average diffusion time $\langle \tau_{diff} \rangle$ = 88 ± 8 µs and an average count rate per molecule <ν> = 2000 ± 280 Hz. Although the values for the fourth detector were different from the other three values, the estimated concentration values (1.3, 1.1, 1.3, 1.4 nM) are again very close.

Table 1 Number of molecules (**N**), diffusion time (τ_{diff}), experimentally observed count rate per molecule (ν), and calculated concentration (C) measured with the four CMOS-SPADs from a single excitation spot.

TMR	5 nM				1 nM			
OUT #	**N**	τ_{diff} [µs]	ν [Hz]	C [nM]	**N**	τ_{diff} [µs]	ν [Hz]	C [nM]
1	3.4	96	5150	4.0	0.52	86	3770	0.73
2	4.3	110	3420	4.2	0.59	100	2670	0.66
3	3.4	90	4830	4.4	0.7	86	4000	0.97
4	3.2	92	4920	4.0	0.52	88	3900	0.7

The values obtained for **N**, τ_{diff}, ν, C using multiple 2 x 2 DOE excitation (Figure 11) were compared to the respective values using the 2 x 2 CMOS-SPAD for single point illumination. Therefore, measurements on solutions with 1 nM and 5 nM free TMR dye molecule concentrations were made with a confocal set-up without the DOE and associated collimators. The data presented in Table 1 show performances for all four single photon detectors of the 2 x 2 array as for the four detectors operating in parallel. Similar trends for the values of **N** and τ_{diff} were observed for both single point and multiple point illumination. The standard deviation of the TMR concentration, measured with each photodetector, did not exceed 5 % and 20 % precision for 5 nM and 1 nM, respectively. However, the values obtained for the fourth detector are better for single point illumination than for 2 x 2 DOE excitation. In addition, the values for ν using the single point illumination set-up are higher than compared to the values obtained with the multipoint illumination set-up. A possible explanation is that due to the DOE excitation the intensity in each spot was reduced so that, non-optimal excitation of the fluorescent molecules was achieved.

3.3. Conclusions – Parallel FCS with CMOS-Detector Arrays

Parallel FCS measurements with a 2 x 2 Geiger mode single photon APD array produced in a standard CMOS process were presented. The performance of this new CMOS-SPAD was compared to the performance of the commercially available SPCM (Perkin Elmer Optoelectronics, SPCM-AQR-13) by measurements on pure dye labeled nucleotides at two different concentrations.

In the CMOS-SPAD detector measurements no afterpulsing was present, allowing for single photon detection of fast dynamical processes. Additionally, a low dark count rate (40 Hz) was observed. The apparent detection probability of the detector is a factor of 5 – 10 lower then for a conventional APD-SPCM with single photon sensitivity. Since, the measurement statistics do not only depend on time, but also on background and afterpulsing contributions, good results precise to within 5 % after only 5 seconds for the determination of **N** and after 15 seconds for the determination of τ_{diff} were obtained with the CMOS-SPAD at 500 pM TMR concentrations. Despite the lower sensitivity, the potential for integration of these detector elements into a smart detector array with on-chip signal processing (e.g. correlators) makes it extremely interesting for parallel single molecule detection instrumentation and HTS. In addition, the industrial CMOS process allows for low manufacturing costs and full integration of Geiger mode photodetector cells.

Parallel FCS measurements using DOE multi-foci illumination and a CMOS-SPAD detector array were performed. Single biomolecule sensitivity was achieved with the CMOS-SPAD for all four detection volume elements. Due to a reduction in excitation intensity in the DOE-excitation spots and some off-axis aberrations in detection, the collection efficiency of the parallel FCS system was reduced and lower values of ν were obtained. However, measurements showed that comparable concentration values were obtained even when non-optimal illumination, higher dark count rates, or lower count rates per molecule were manifest. This is a very important point for future development of the parallel FCS instrumentation since a high integration of the detectors might lead to complications with the source-sample-detector alignment, which, as we observed above, did not affect the outcome of the concentration determinations made with FCS measurements. Here, the CMOS-SPAD gave reliable results in the nM regime (the range where most of the FCS measurements are performed presently). Additionally, precision to within 5 % for the determination of **N** was obtained even after only 5 seconds measurement time, making the CMOS SPAD

suitable for most biological applications where relative differences in concentration have to be determined.

However, measurements at lower concentration would benefit from a higher collection efficiency and a larger active area of the detector. At the same time, optical strategies should be found to improve the energy collection for the small active area of the detector. In order to broaden scope of the applications in molecular biology and to implement this detection scheme in these new applications, the detector sensitivity should be shifted to the red region too. Moreover, the assumption that the equation $S/N \sim \sqrt{x \cdot \mathbf{N}}$ becomes valid with multiple foci excitation and detection has still to be followed up in order to see that a real improvement can be achieved. Again, the capability of the CMOS fabricated detector arrays to include on-chip processing would for this purpose be highly advantageous.

4. Gene Expression Analysis (paper V)

A novel method for gene expression level analysis within a cell has been developed. From the expression profile of well-defined genes it is possible to conclude phenotype, function and response to the environment of the cell. This is of major importance in disease diagnostics, for new target identification, drug identification and optimization, and monitoring of clinical trials.[109-112] In addition, knowledge about the gene expression level can potentially provide clues about regulatory mechanisms, biochemical pathways, and broader cellular functions. Various techniques are used for the analysis of the gene expression level. The micro-array technique using high-density oligonucleotide chips[113,114] or cDNA arrays[115,116] enables simultaneous analysis of several thousands of genes and is commonly used for research and commercial drug discovery. Although this technology has an enormous scientific as well as industrial potential there are still some limitations with respect to the data thus obtained. The regulated genes can be identified reliably with both the oligonucleotide and cDNA arrays, but the degree of regulation can differ from measurement to measurement or be inaccurate.[117] In particular, many results obtained from measurements with both cDNA arrays or oligonucleotide chips showed a poor correlation with each other.[118,119] Additionally, the reproducibility of both techniques is poor without signal optimization for each individual probe-target pair.[120] Until now, the most sensitive and precise method for the quantification of mRNA molecules has been the real time PCR (RT-PCR) method. However, this is a complex technique which also has substantial problems associated with reproducibility and specificity.[121-124]

One novel gene expression profile detection method described herein is based on single spot Fluorescence Cross Correlation Spectroscopy (FCCS) analysis (for more details on FCCS also see chapter 5). Due to the high sensitivity of the dual-color FCCS analysis method no amplification steps are needed and the number of gene targets was determined by directly analyzing the sample. Gene target specific red and green dye-labeled DNA probes were designed and hybridised to the gene encoding DNA sequence. The sample was then measured with two-color FCCS and from the amplitude of the resulting cross-correlation curve, the number of gene targets was calculated. Given the originally amount (µg cDNA in the sample), the target copies of interest per µg cDNA were calculated.

4.1. FCCS – Theory

In FCCS a positive response results only if the signal fluctuations coming from two different signals of whatever origin reach the detector unit simultaneously. In the case of dual-color cross correlation the signal of one dye is compared (correlated) to the signal from another dye. Therefore solely biomolecules with two complementary dyes (in this case red and green), which emit at two different wavelengths simultaneously, contribute to the cross-correlation signal. Molecules (probes) containing only one dye cannot be observed since their motions are uncorrelated in time.[43] Following Rigler *et al*.[44] I introduce here the theoretical formulas needed in order to analyze subsequent FCCS measurements. Using $I_r(t)$ and $I_g(t)$ to represent the intensities corresponding to the red and green emission wavelengths, respectively, and $\delta I_r(t)$ and $\delta I_g(t)$, respectively, to representing the deviations from these mean intensities (i.e. fluctuations), the normalized cross-correlation function of two intensity fluctuations can be expressed as follows

$$G_{gr}(\tau) = \frac{< \delta I_g(t) \cdot \delta I_r(t+\tau) >}{< I_g(t) >< I_r(t) >}, \qquad (8)$$

where the brackets < > denote the time average and τ is a constant time-delay. Given the autocorrelation function at the time $t = 0$ for the red and green fluorescent molecules, respectively, $G_g(0) = 1/N_g$ and $G_r(0) = 1/N_r$, the number of molecules labeled with both dyes can be calculated using

$$N_{gr} = \frac{G_{gr}(0)}{G_g(0) \cdot G_r(0)} = G_{gr}(0) \cdot N_g \cdot N_r \qquad (9)$$

4.2. Specificity of Assay, Calibration Curve – Experimental

4.2.1. FCCS Set-up

A sketch of a dual-color multi-focal excitation and detection set-up is displayed in Figure 9 and described in chapter 5. The set-up in use has single point illumination and detection, which means that no DOEs and associated collimators were inserted into the light path and only two avalanche photo diodes, one for the red and one for the green channel, were used.

4.2.2. Gene Specificity of Assay

In order to determine the gene specificity of the assay, a β-actin depleted total cDNA sample was prepared. Therein, all the actin molecules were specifically bond to beads and removed from the sample. The decoupled sample contained less than 5 % of the actin molecules originally present. In the following, two gene specific β-actin probes (red and green) have been added to 100 ng total cDNA and 100 ng β-actin depleted total cDNA each at a concentration of 2 nM. In order to avoid any unspecific interactions, the hybridization was performed under temperature-controlled conditions. The two samples were measured with FCCS and the cross-correlation curve was recorded. Figure 12 presents a comparison between the β-actin hybridization measurements of the original (total cDNA), the β-actin depleted and the background sample (the probes only), respectively. The cross-correlation signal for the depleted sample is within the background contributed by the free probe pairs (spill-over) corresponding to less than 10 % of the response of the original sample, a result which therefore clearly demonstrates the specificity of this method. The β-actin gene is a so-called housekeeping gene and is present in the cell at a constant and rather high concentration. It was chosen for the specificity test because the difference in cross-correlation amplitudes between the depleted and non-depleted cDNA samples differs more than it would for genes that are less expressed in a cell.

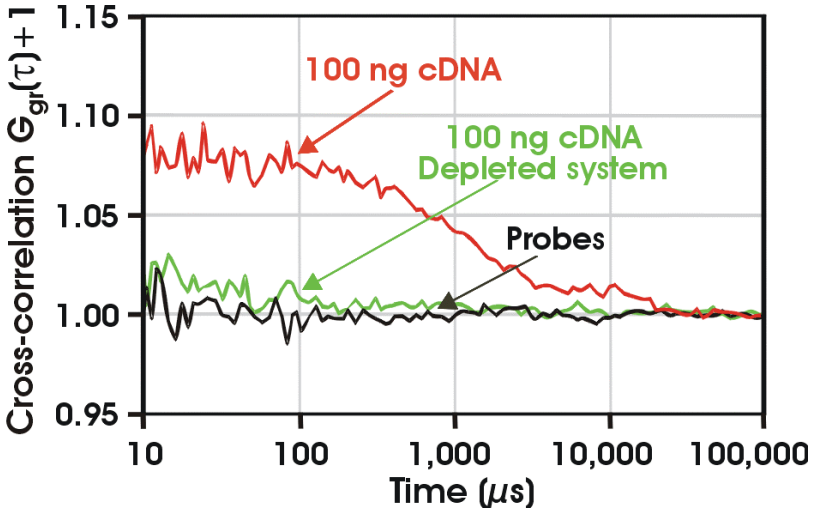

Figure 12 Cross-correlation curves obtained upon hybridization of 2 gene-specific actin probes to either 100 ng total cDNA or 100 ng β-actin depleted total cDNA.

4.2.3. Calibration Curve

Absolute and accurate quantification requires the generation of a calibration curve, and this was measured for each selected gene. At a given probe concentration, different amounts of gene specific single stranded (ss) cDNA were hybridized to the selected probe pairs. Figure 13 (left) shows cross correlation curves obtained for ss PGK1 cDNA. Values of N_{gr} were plotted on the ordinate axis against the target concentrations that have been used in the experiment. Because the two values are proportional to each other, a calibration curve (Figure 13,right) was obtained, and used as standard curve for the determination of the absolute number of gene copies.

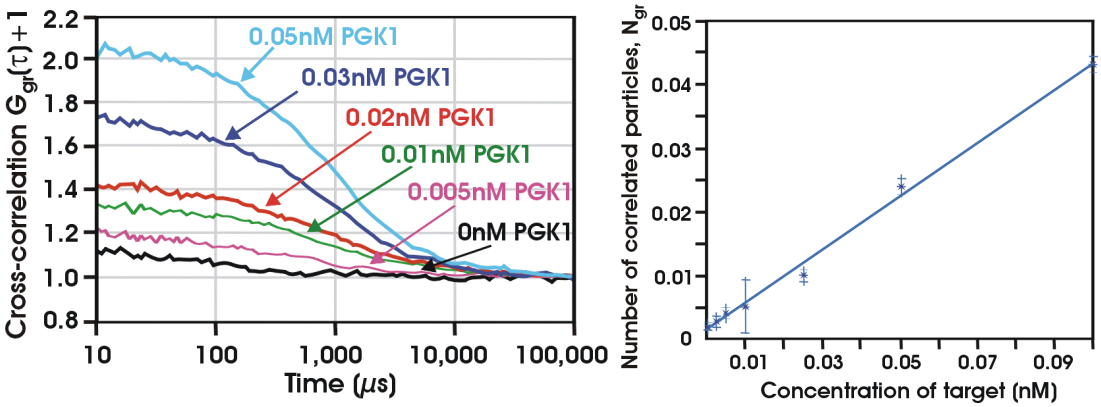

Figure 13 (left) Cross-correlation functions obtained using 5', 3'- bi-labeled green and 5'-red-labeled probes with a final concentration of 0.1 nM and ss PGK1 cDNA concentrations of 0.05 nM, 0.03 nM, 0.02 nM, 0.01 nM and 0.005 nM. Using the resulting numbers of cross-correlating molecules, N_{gr}, a calibration curve (right) was calculated. The number of molecules, N_{gr}, is a function of the ss cDNA concentration from 0.005 nM – 0.1 nM. The measurement time was 240 s at 50 °C. Each data point is the average of three independent measurements. The error bars illustrate the 95 % confidence interval for N_{gr}. The slope of the calibration curve is a direct measure of the binding efficiency of the probe pair to the specific gene under the given experimental conditions.

4.3. Gene Quantification in HL-60 cDNA – Results

In order to determine the concentration of selected genes within a biological sample hybridization experiments were performed wherein the gene-specific cDNA was replaced by total cDNA (100 and 200 ng each) of HL-60 cells. Utilizing the previously established calibration curve (Figure 13, right), the particle numbers, N_{gr}, obtained from the cross-correlation curve were translated into a concentration for each gene within the biological sample. Finally, this concentration was used to calculate the copies/µg of cDNA. With the FCCS based gene expression assay various genes in high, medium and low abundance were quantified. For highly abundant genes, typical values (copies/µg of cDNA) of (4.3 ± 1.3) x 10^9 for S19, (7 ± 3) x 10^8 for tuba and (5.4 ± 1.3) x 10^9 for EL-1 were obtained. The uncertainties associated with the ex-

pression levels are based on a 95% confidence interval. For genes of medium and low abundance the following number of copies/µg of cDNA were measured: $(2.4 \pm 0.7) \times 10^8$ for DNAbp, $(2.4 \pm 1.1) \times 10^8$ for RAB1 $(5.7 \pm 0.5) \times 10^7$ for PGK1 and $(1.3 \pm 0.8) \times 10^7$ for p65. Linear dynamic range of analysis exceeds 3 orders of magnitude (10^7-10^{10} copies/µg cDNA).

4.4. Conclusions – Gene Expression Analysis

A new analytical method to measure gene expression level, which quantifies genes in absolute numbers by determining the number of genes carrying two labels (probes), and with amplification neither of the sample nor the detected signal, has been presented. A calibration curve was established to provide a quantitative measure for the efficiency of probe-target binding, which can be below 100 % when reduced probe binding occurs due to secondary structure formation of the target. With the calibration curve, a correction factor was obtained and quantitative evaluation of gene expression level over a range of at least three orders of magnitude was possible. Other methods like RT-PCR allow the quantification of selected genes in absolute numbers too. The RT-PCR concept is based on the determination of C_t values (where the fluorescence signal reaches the point that is statistically significant above background)[125] whereas the assay presented here directly determines the number of double-labeled molecules (N_{gr} values). In both cases C_t or N_{gr} are translated into the number of target copies per µg cDNA with the help of a calibration curve, but in case of RT-PCR assays the generation of a standard curve has to be repeated for every new quantification to ensure accurate reverse transcription and amplification profiles.[124] The presented new technology requires that a calibration curve is determined only once for each specific gene. Then, the determination of the copy number per µg cDNA can be based on this calibration curve by simultaneous measurements of a limited number of defined controls. In the present stage 10^6 cells are required to detect genes in low abundance within a measurement volume of 1 µl. As no amplification is involved in the whole procedure, the next step of reducing the sample amount is to decrease the hybridization volume. By reducing the well volume to, for instance, 234 nl, the concentration of all reagents could be kept at the same level, which is crucial for the reaction kinetics. In future, new detection strategies can be used to increase the fluorescent event rate of the double-labeled molecules, especially in the regime of low gene abundance. This can be done with, for example, a multiple parallel confocal dual-color detection set-up, based on DOEs. More about this subject will be presented in the next chapter.

5. Parallel Dual-color Cross-correlation (paper VI)

As shown in chapter 4, dual-color FCCS allows for the detection and analysis of labeled biomolecules at ultra low concentrations.[11] FCCS improves the S/N in reaction schemes with fluorescent labeled probe substances, where, in the case of extremely low concentrations of target molecules still a large excess of unbound probes may still be present. The experimental set-up the of dual-color cross-correlation experiment is based on the fine spatial resolution of the confocal scheme[92] and spectrally well-separable fluorescent dyes that are both attached to the target molecule. The first experiment on the single molecule level was realized with a system of dual-labeled complementary DNA oligonucleotides hybridised to each other.[43,126] Later on, cross-correlation analysis was used for diagnostic purposes[127] and to monitor nucleic acid or protein interactions.[44,128] Additionally, Kettling *et al*.[129] employed cross-correlation for in-vitro analysis of enzymatic kinetics. In further technical improvements involving two-photon excitation, the excitation volume element as well as the measurement time was decreased and the feasibility of this method for cellular analysis shown.[130] Instead of recording the full cross-correlation function containing all dynamic information about the fluctuation of molecules, a simplified data analysis algorithm has been developed, concentrating only on the fluorescence fluctuations in two different spectral ranges that correlate in each of them for a given observation volume. This so-called coincidence analysis[131] simplifies the data processing procedure and consequently reduces the measurement and analysis time. HTS analysis, drug discovery and development, as well as diagnostic tests in medicine, can be achieved in small sample volumes thereby reducing costs.[132,133] Here, the introduction of microarray techniques reduced the sample volume significantly (to 1 µl per well or sample droplet)[134] and established a useful technological platform for fast parallel analysis in life science experiments.[97,98,135] However, the sample quantity (concentration) is often still in the nM regime to increase the rate of fluorescent events and to assure a good statistical precision. Moreover, external perturbations (e.g. probe scanning or flowing sample streams)[127,131] were applied to increase the number of events at very low concentrations or for slowly diffusing molecules. This technique is commercially used for e.g. HTS.[136] However, in this case fewer photons per passage time (through the excitation volume) are released from the molecules of interest and subsequently detected by the detector, which is of disadvantage.

In order to increase the number of detectable photons per passage time for low concentration solutions and slowly diffusing molecules, multiple fixed dual-color cross-correlation excitation volume elements were generated by DOEs and detected by avalanche photo diodes. This configuration increases the measured fluorescence event rate artificially, thus retaining the maximal emitted photons per molecule without any movements of the system. The performance of this multiplex FCCS system, consisting of 2 x 2 DOE generated cross-correlation foci and four SPCM-APDs, was characterized with a self-manufactured PCR-product, which was labeled with both red and green dyes.

5.1. FCCS Theory for Cross-talk and Concentration Determination

In accordance with chapter 4.1. the FCCS theory is modified and account for cross-talk contributions. Since the emission spectrum of Rhodamine Green (RhGreen) is very broad, substantial fluorescence can be detected in the red channel. This phenomena is called cross-talk, and the cross-correlating amplitude can be written as follows[44]

$$G_{gr}(0) = \frac{N_g q + N_{gr}(1+q)}{\left[N_g + N_{gr}\right]\left[N_r + N_g q + N_{gr}(1+q)\right]}.$$

This equation can also be expressed in the number of cross-correlation molecules and thereby resembles equation 9:

$$N_{gr} = \frac{G_{gr}(0)}{G_g(0)\cdot G_r(0)\cdot(1+q)} - \frac{N_g \cdot q}{(1+q)}. \qquad (10)$$

Here, $G(0)$, denotes the amplitude of the respective autocorrelation curves (green, red and red/green), $q = Q_B^R / Q_R^R$, whereby Q_R^R and Q_B^R are the fluorescence detection efficiencies expressed in relative photon counts per second for red excitation (lower index) and red emission detection (upper index) and blue excitation and red emission detection, respectively. Since $Q_B^G = 1$ and $Q_R^G = 0$ do not contribute significantly to equation 10, both terms have been neglected. In order to calculate concentrations in the cross-correlating sample, the size of the cross-correlating detection volume element has to be determined as well:

$$V_{gr} = \pi^{3/2} \frac{\left(\omega_g^2 + \omega_r^2\right)}{2} \sqrt{\frac{\left(z_g^2 + z_r^2\right)}{2}}, \qquad (11)$$

with ω_g, ω_r, z_g and z_r being the 1/e^2 half-axes of the Gaussian distribution of the green and the red detection volumes, for each, respectively.

5.2. Set-up and Samples – Experimental

5.2.1. Multiple and Single Spot FCCS Set-up

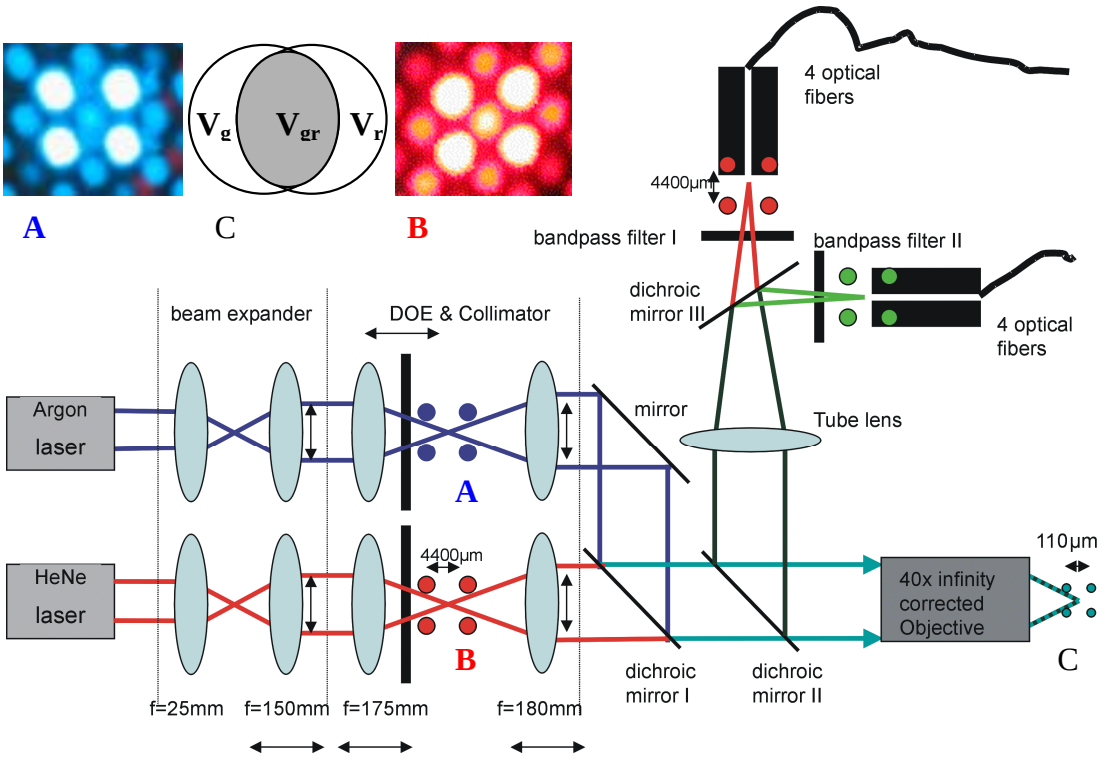

Figure 14 For details about the set-up see text. The generated 2 x 2 pattern for each laser is displayed at the top. A schematic of the overlap of the excitation volume elements is presented in between the patterns. For the Gene Expression Analysis experiment (chapter 4), the DOEs were not inserted and only two (one for red and one for green) glass fiber connected avalanche photo diodes were used.

A schematic of the parallel fluorescence cross-correlation spectroscopy (pFCCS) set-up is shown in Figure 14. A 488 nm laser line of an argon multi-line laser and a 633 nm Helium-Neon laser line were both expanded 6x by individual expanders. Both beams were passed through individual DOE-collimator combinations to generate the desired two 2 x 2 multi foci beams (Figure 14 (top)). An aperture was placed after each DOE to block the second-order-generated diffraction pattern. The zero order was suppressed by the design of the DOE. Thereafter, both beams were combined by a dichroic mirror (I, Chroma, 620dcxr) and sent into the back port of an inverted microscope (Olympus IX 70). Here, the two 2 x 2 excitation beams were reflected by a second dichroic mirror (II, Chroma, 488/633/1064) and directed into a 40x water immersion objective (Olympus, ICS-UAPO40X/340, NA=1.15, cover glass corrected), which focused the superimposed laser beams into the sample solutions The resulting dual-color fluorescence emission was collected by the same objective, transmitted by

the dichroic mirror II into a tube lens which focused the emission onto optical multimode fibers. In-between, the emission was split into its green and red fluorescent components by a third dichroic mirror (III, Chroma, 630dcxr) and filtered by bandpass filters (Chroma, 685/70 (I) and D540/60 (II)) to suppress Rayleigh- and Raman-scattered light. The diameters of the optical multimode fibers, acted as pinholes, which were different for the green (50 µm) and red (62.5 µm) fluorescence emission. The multimode fibers were held by an in-house built 2 x 2-x-y translator that allowed for independent spatial adjustment of all fibers. The fiber outputs were connected to a four-channel APD array prototype (Perkin Elmer Optoelectronics, SPCM-AQ4C) or to single APDs (SPCM-AQR-14). The logical TTL signals were then transferred to a PC-based correlator (ALV-5000), which computed and displayed the photon count rate and correlation curves.

5.2.2. Samples

The fluorescent dyes used for the autocorrelation analyses were Rhgreen and Cy5. The probes used for cross-correlation measurements were partially double stranded (ds) DNA molecules (99nt). Both probes (probe I and probe II) had two different double-labeled fluorescent primers (one with 5’ RhGreen / 3’ RhGreen and the other with 5’ Bodipy 630 / 3’ Bodipy 630) hybridized to them.

5.3. Characterization of Multiple DOE Generated Dual-color Excitation Spots – Results

5.3.1. DOE-Generated Autocorrelation Curves

Figure 15 (left) shows two representative autocorrelation curves (normalized) of labeled nucleotides in nM concentrations, with parallel red (633 nm) and blue (488 nm) DOE generated excitation foci. As can be seen, the diffusion time for the Cy5-labelled molecules is longer. This is because of the bigger diffraction limited volume element for the red excitation wavelength ($2 \cdot \omega_{xy} \sim \lambda / 2 \cdot NA$, with *NA* being the as numerical aperture of the objective). The signals of three individual cross-correlating detection volume elements were recorded, simultaneously, with the three available hardware correlators. The experimentally obtained autocorrelation curves were fitted with the analytical expression (Equation 2) for one component (species).

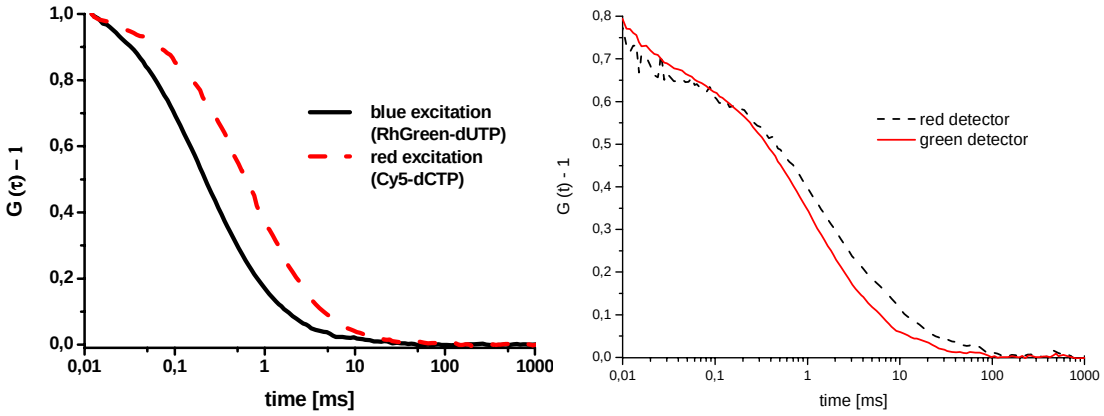

Figure 15 (left) Normalized representative autocorrelation functions for DOE generated foci. The dotted autocorrelation curve originates from RhGreen-dUTP, the other from Cy5-dCTP. (right) Cross-talk and normal autocorrelation curve of RhGreen-dUTP for the red and green detection channels, respectively. The amplitudes are similar only the diffusion time differs, which means that the two detectors (for red and green) image approximately the same volume. The diffusion time for the red detector is longer, which is explained by a bigger pinhole (62 µm instead of 50 µm) in the red channel.

The results of these measurements are displayed in Table 2 (on the next page). The most important parameter for biomolecule analysis is the concentration of molecules present in the sample. As shown in Table 2, the concentrations of the molecules measured in the three detection volume elements were almost identical; C = 1.4 ± 0.1 nM for the Cy5-dCTP and C = 6.8 ± 0.7 nM for the RhGreen-dUTP (concentrations were calculated with $C = \mathbf{N} / V$, wherein $\mathrm{V} = R \cdot (4\pi\tau_{diff} D)^{3/2}$ is the detection volume element). Different Gaussian intensity distributions could be excluded as the cause of deviations in **N,** τ_{diff}, and ν, because we know from previous work that the 2 x 2 fan-out DOE foci exhibit equal intensities.[100] In addition, the biomolecule concentration in the droplet is the same for each spot and thereby, the results should all be the same. The only explanation for the differences in **N,** τ_{diff}, and ν is obviously due to aberrations in the excitation beam that could not be prevented. However, alignment of the DOE could be performed sufficiently well to result in consistent concentration determinations, $C = \mathbf{N} / V$. Precision associated with average concentrations is less than 10 %, although the relative standard deviation for other parameters, like diffusion time, τ_{diff} , and number of molecules, **N**, is more than 25 %.

Table 2 Experimentally obtained parameters for DOE-generated foci. In the top row, the detection foci (I-III) are denoted for the red (**cy5**) and the green (**rg** = Rh-green) channels. **N** denotes the average number of molecules present in the observation volume element, τ_{diff} is the radial diffusion time of the molecules, and ν is the experimental observed count rate per molecule.

	f I cy5	**f II cy5**	**f III cy5**	**f I rg**	**f II rg**	**f III rg**
N	3	2,5	4	12	12	12
τ_{diff} **[ms]**	0.37	0.36	0.46	0.20	0.20	0.18
R	3	3	3	7	7	7
ν **[kHz]**	83	84	58	48	52	73
C **[nmol/l]**	1.5	1.3	1.4	6.4	6.4	7.5

5.3.2. Cross-talk and Overlap of the Excitation Volume Elements

In order to get the highest possible overlap of the two (red and green) excitation volume elements the cross-talk signal of freely diffusing RhGreen dye labeled molecules (red detection channel) was compared to the normal fluorescence signal of the dyes (green detection channel). Due to their broad emission, green dye spectra emit light in the red region and an autocorrelation curve can be recorded in the red as well as the green channel. When equal amplitudes are obtained, the number of molecules in both detection volume elements is the same and the pinholes for the green as well as for the red channel image the same excitation spot. In order to achieve a good overlap, the DOE excitation foci were adjusted until the signal in the red channel was optimized. In Figure 15 (right), a representative non-normalized autocorrelation curve for blue excitation and green fluorescence as well as the red fluorescence of the green dye (cross talk) is displayed. The slightly longer diffusion time for the red detection channel accounts for the slightly bigger pinhole that has been used (62 µm instead of 50 µm in diameter).

5.3.3. Multiple Dual-color Cross-correlation Analysis

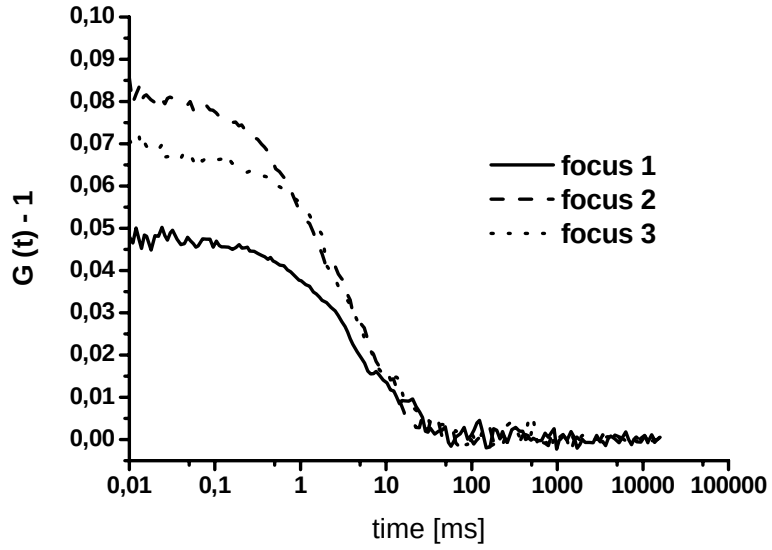

Figure 16 The three cross-correlation curves were obtained simultaneously from three different dual-color foci for probe II.

Figure 16 shows three dual-color DOE-generated cross-correlation curves of freely diffusing double-labeled PCR-product molecules. Each PCR-product (probe I and II) was dispersed in a single droplet onto a cover glass at a total concentration of around 0.1 nM and measured separately. In each case, the measurement time was one minute. The resulting cross-correlation curves were fitted with the analytical expression of a single component model (Equation 2) to obtain the cross-correlation amplitude value, $G_{gr}(0)$. The autocorrelation function of each of the three foci for the red and the green channel were recorded and analyzed with the same function to determine the number of red- and green-labeled molecules ($G_g(0)-1=1/N_g$ and $G_g(0)-1=1/N_r$, respectively). The number of cross-correlating molecules, N_{gr}, was calculated using equation 10, with Q_R^R and Q_B^R having been previously determined to be 1.6 and 0.02, respectively, q equals 0.0125. Given estimated parameter values, such as the ratio between the axial and the radial dimensions of the detection volume element, R, the diffusion time of the free dyes, τ_{diff}, and the cross-correlation detection volume element, V_{gr} (Equation 11), the concentration was calculated for each dual-color detection volume element. The results are summarized in Table 2. The cross-correlation curves for the three foci were not equal in amplitude (differences > 60 %), but the concentrations from all three spots, however, turned out to be similar and only had a relative standard deviation of approximately 20 % (independ-

ent of the probe). The differences in amplitude gave us a clear indication that the overlapping of the red and the green excitation foci and/or the fluorescence imaged by the red and the green pinholes were not the same for all three spots. However, by taking the volume elements, V_{gr} (equation 11), for the different overlapping spots into account and correcting for the variations in the autocorrelation amplitudes $G_g(0)$ and $G_r(0)$, these differences were compensated.

Table 3 Experimental determined concentrations for three spots (f I, f II and f III) for two different biological samples (S I and S II). STD denotes the standard deviation of the three independent measurements.

Sample	f I	f II	f III	Average (STD)
S I [pM]	56	80	65	67 (12)
S II [pM]	71	114	97	94 (22)

5.4. Conclusions – Parallel FCCS

A multi-focal dual-color cross-correlation spectroscopic system using two 2 x 2 fan-out DOEs with single biomolecule sensitivity was developed. The parallel system showed uniform intensity in all four foci and almost invariant results (i.e. for **N**, *C,* τ_{diff} and ν) for single-color excitation and detection. For dual-color cross correlation analyses, larger variations in the amplitude of $G(0)$, but acceptable variations in concentration were observed. With this parallel focal dual-color cross-correlation set-up, the concentrations of double-labeled DNA-molecules in the pico-molar regime were determined with a relative standard deviation of 20 % for the different foci. Although a cross-talk signal was present, the cross-correlation signal of double-labeled DNA-molecules could easily be distinguished. Implementing better fine adjustment capability (e.g. micrometer screws) into the 2 x 2 fiber holders should decrease the variations in amplitude and allow for more consistent values. Thereby, normal cross-correlation analytical precision (to within 5 %) could be achieved for each focus. Combining information from all four foci could enable decreased measurement times or lower rare event detection limits even further. Future applications involving HTS and concentration determinations for small concentrations and/or slow diffusing biomolecules (e.g. gene expression analysis, chapter 4) can profit from this parallel ultra-high sensitivity and real time dynamical cross-correlation fluorescence scheme.

6. Single Molecule Detection in Flow (papers I, VII & VIII)

In order to efficiently take advantage of SMD,[3-5,22,92,137-140] improved techniques for manipulation, separation and detection of small quantities of diluted reagents for fields such as biotechnology[141,142] have to be designed. Microfluidic systems are an ideal platform for developing ultrasensitive and less time consuming[143] analytical methods (see chapter 2). One aspect of microfluidic-based systems is the fast, efficient detection and identification of interesting molecules in flow that can be performed with laser beams.[6,42,138,142,144] Confocal spectroscopy has an unique advantage due to its high *S/N* ratio of up to1000 for the detection of single molecules even in rapid flows (up to 10 mm/s). In order to achieve a high *S/N* ratio the detection volume has to be small (< 1 µm).[92] To detect molecules of interest in such small detection volume elements in channels of a few µm in size (~ 10 – 100 µm) attempts to guide the molecules through the detection volume (~ 1 µm) have to be undertaken. For this purpose, sheath flow or hydrodynamic focusing has mainly been utilized,[10,49,145,146] enabling a faster analysis and in the same cases improved analytical selectivity. The probability of identifying a molecule correctly depends, in addition to a chosen threshold value on the overlap of the burst-size distribution for the background and for the molecules of interest, respectively. Assuming that all the molecules of interest passing through the detection volume element have an average S/N ratio of 10, a 3σ threshold (99.9 % confidence) would result in a molecular detection efficiency of 80 %. Obtaining a molecular detection efficiency of > 95 % requires a S/N ratio of 55.[147] Different approaches towards single molecule detection in flow have been undertaken by several groups[12,147-151] trying to reach such a high detection efficiency. However, the highest molecular detection efficiency to date has been achieved for TRITC molecules by Goodwin *et al*.[53] and exceeded 90 %. Here, the dyes were eluted from a 1 µm inner diameter capillary and focused by sheath flow. In this chapter investigations of single molecule detection in commercially available microstructures were made. In the structures described, background scattered light was present, which led to a lower S/N ratio for the molecules than in droplet experiments. However, different approaches like elliptical line focus or Polymethylmetacrylate (PMMA) microstructures were utilized in order to screen or simply detect highly fluorescent molecules in a biological sample. In addition, experiments for the selection or fractionation of single biomolecules of interest from huge chemical or biological libraries were performed and the results are presented.

6.1. Set-up – Experimental

The experiments were mainly performed with a single confocal volume element set-up. First, a green Ar-laser (515 nm) has been focused into the sample (see chapter 1). Then the Ar-laser was substituted with a red HeNe laser (633 nm) that was expanded in one direction into a line focus (Gaussian curtain) to increase the detection probability. The excitation line focus was consequently imaged onto a slit instead of a round pinhole.

6.2. Single Molecule Detection Experiments – Results

6.2.1. Detection of TMR-dUTP in Flow in Silicon-Glass-Microstructures

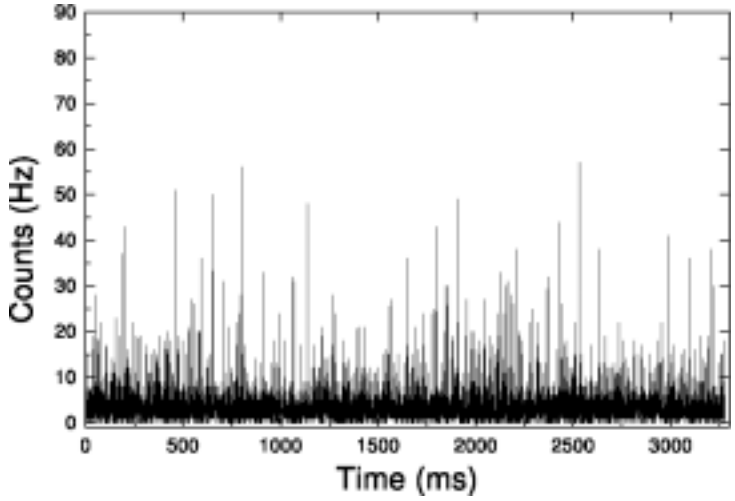

Figure 17 Single molecule bursts from inside a 50 x 50 µm^2 microchannel with an applied flow of 10 mm/s.

Commercially available silicon-glass-microstructures were used to detect single TMR-dUTP molecules in flow. A great emphasis was placed on the effective integration of microfluidic devices into available flow systems. Thereby, better reproducibility in terms of flow velocity and sample priming was achieved. However, the S/N ratio was also influenced by scattering and autofluorescent light contributions from the window material of the channel. This problem is known and has already been investigated by Wabuyele *et al*.[33] for polymer microstructures. Glass microstructure devices have been investigated by Fister *et al*.[149] Here, a S/N ratio of roughly 10 was achieved for a flow velocity of approximately 0.5 mm/s. With such flow velocities, a near optimal number of photons per passage time can be obtained, since the flow rate is in approximately the same range as the diffusion velocity of single molecules. In order to achieve a higher throughput, the correct combination of fluidic-controlled molecular transport through the detection volume element with a concomitant in-

creased flow velocity well above the diffusion velocity of the molecules of interest has to be found, because letting the molecules pass in a higher flow velocity through the detection volume element consequently decreases the count rate per molecule per passage time. The signal of TMR-dUTP nucleotides under conditions of purely diffusive transport was compared to the signal obtained for TMR-dUTP nucleotides in liquid with a flow velocity of 10 mm/s (Figure 17). Here, a S/N ratio of 10 and 4 for diffusion and flow, respectively, were obtained in the silicon microstructures, even though scattering background light contributed to the signal. For flow velocities of approximately 5 mm/s (as is used for applications like single molecule DNA degradation in flow) a S/N of 7 was achieved (data not shown). This is, however, far away from the S/N ratio of 55 that should be achieved in order to determine passing molecules with a detection probability of more than 95 %. Therefore, other strategies such as using different microstructure material, different wavelengths or molecules with higher count rates must be pursued.

6.2.2. Single Molecule Detection with a Gaussian Curtain (Elliptical Line Focus) – Amyloid β-peptide Screening

The detection of large and slowly diffusing molecules undergoing purely Brownian motion in liquid is difficult. For low concentrations it might even be impossible to measure and quantify the number of molecule in the sample in a reasonable time. In particular, the detection of large aggregates of a sub-nM solution of, for instance, Amyloid beta (Aβ) peptides (e.g. those implicated in Alzheimer's diseases pathology)[25,127,152,153] in a micrometer-sized focus, can take several thousands of seconds for freely diffusing molecules. The detection time for diffusion-controlled reactions is governed by the recombination rate, $k_R = 4\pi D R_C \mathbf{N}$, of the bigger molecule in the laser focus,[42] where R_C is the radius of the sphere-like laser focus volume element. Therefore, fluidic-controlled transport of biomolecules through a detection volume element increases the recombination rate by several orders of magnitude (dependent on the flow velocity) and thereby paves the way to a novel diagnostic method for Alzheimer's disease. In order to increase the recombination rate, $k_{R,}$ even further, a bigger detection volume element was designed, thus increasing Rc. The so-called Gaussian Curtain (elliptical line focus) covered almost half of the cross section in the microfluidic channel (Figure 18). Comparing the elliptical line focus volume element (20 x 5 x 1 μm^3) with the commonly used spherical excitation focus (5 x 1 x 1 μm^3), the overall detection efficiency in terms of detected molecules per detection volume element is theoretically increased by a factor of 20. However, the background is in-

creased by approximately the same factor as well, thus the S/N ratio for this detection configuration would not produce an inherent advantage to the commonly used round spot configuration if not for Aβ-peptides aggregates samples. Here, each peptide is labelled with one dye and aggregates made up of many peptides exhibit a high fluorescent burst signal that can be discriminated against the background in an elliptical line focus, in as much as the aggregate signal increases, but the background does not.

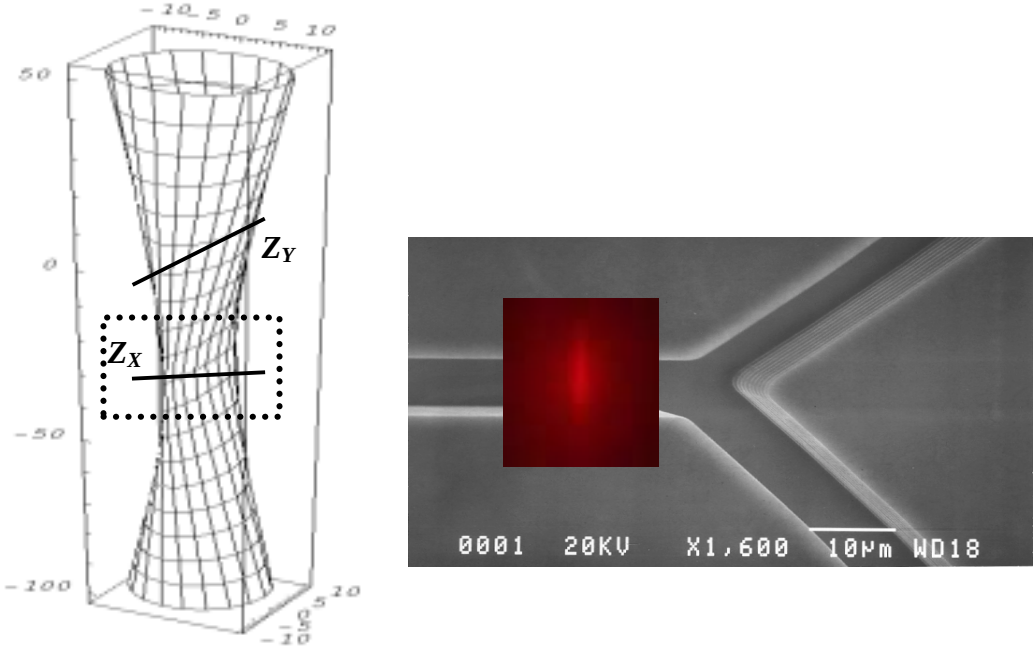

Figure 18 Elliptical line focus (left). Scanning electron microscopy picture of a 10 x 10 µm^2 dry-etched microchannel in silicon with a bonded glass roof (right), in addition, a fluorescence picture of the elliptical line focus (magnified) in Cy5-dCTP solution (10 nM) is displayed.

A typical signal trace of a sub-nM Aβ-peptide aggregate solution in flow is shown in Figure 19. As a comparison, the insert (background) shows a gel filtered Aβ-aggregate solution. In the screening experiment, a flow velocity of 0.2 µl/min was applied in a 50 x 50 µm^2 silicon channel (Figure 2), which corresponds to a flow velocity of 3 mm/s in the middle of the channel. Over a period of 350 seconds more than 100 aggregates could be identified. In comparison to that, for a measurement on sub-nM Aβ-peptide aggregate solution (for purely diffusion throughput), less than five bursts were recorded over a measurement time of two hours using the normal round excitation focus of the size of 5 x 1 x 1 µm^3. With the Gaussian Curtain method, a through-

put increase of 2 – 3 orders of magnitude was achieved, although the background (40 kHz) increases by a factor of 20 due to the larger detection volume element (Figure 19). On the other hand, the single Aβ-peptides aggregates exhibit photon bursts of 60 - 80 kHz and a S/N of 2. This shows that the elliptical line focus detection set-up allows for efficient throughput analysis although a low detection efficiency (less than 10 %) was achieved. This is, however, possible when not every molecule present in the sample needs necessarily be detected. For applications such as single molecule selection and single molecule DNA sequencing (see below), the background has to be reduced strongly and the S/N increased to achieve higher detection efficiencies.

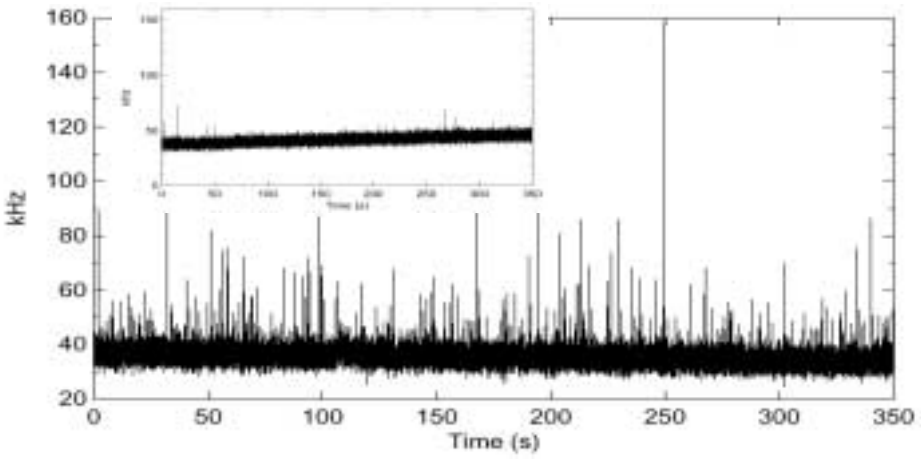

Figure 19 Bursts signal from a pM Aβ-aggregate solution (given a bin size of 6 ms). The inset shows results from a measurement on a gel-filtered Aβ-aggregate solution.

6.2.3 Single Molecule Selection – Screening of Libraries

Experiments towards the up-concentration of bimolecular or chemical libraries have been pursued. The idea where biological evolution can be simulated to create an enormous diversity of compounds, which carry a common scaffold, but have combinatorial inserts with different functional properties, has changed the scenario of drug discovery. Molecular libraries have been developed as a widespread tool for the discovery of molecules with certain properties,[154-159] for instance, binding to a cellular receptor, blocking of dimerisation. The last decade has seen dramatic developments in the available technologies for cloning, and the expression and selection of antibodies and other affinity molecules with a broad range of specificities resulting from the creation of very large libraries of cloned polypeptides (1 – 100 million members or more). Here, several different strategies for selection have been described, for example, with soluble biotinylated antigens captured by using streptavidin-coated mag-

netic beads,[160-162] coated tubes or wells,[163] columns,[164-166] or simply by the selection of antigens with cells.[167-169] Different enrichment factors were reported with a normal average of around 10 - 1000[170,171] per selection cycle. However, in order to fully utilize the potential of these large libraries, improved selection strategies, with a reduction in non-specific binding, would be most desirable. In pursuit of this goal, a selection method based on either an elliptical line focus or DOE generated multiple foci curtain and a Y-shaped microstructure is proposed (Figure 2). For this method, the microfluidic structure has three legs; one leg is named ‘inlet’ (single leg to the left) and the other two are named ‘drain’ and ‘select’ (Figure 20). The idea is that the sample is inserted into the ‘inlet’ leg and pushed through by a syringe pump at a certain constant velocity to the waist leg on default. The detection focus is positioned in the middle of the channel and a labelled molecule of interest passing the detection focus generates photon bursts. In order to select the detected molecule into the ‘select’-leg of the microstructure, high-speed micro dispensing valves (VHS) is inserted into the waist flow behind the microstructure. If the photon burst of the detected molecule exceeds a certain threshold, the valve will be closed for a short period of time (< 1 ms) and the molecule of interest will be directed into the ‘select’-channel. Later, the contents of the ‘select’ channel will be extracted and amplified by standard biological methods.

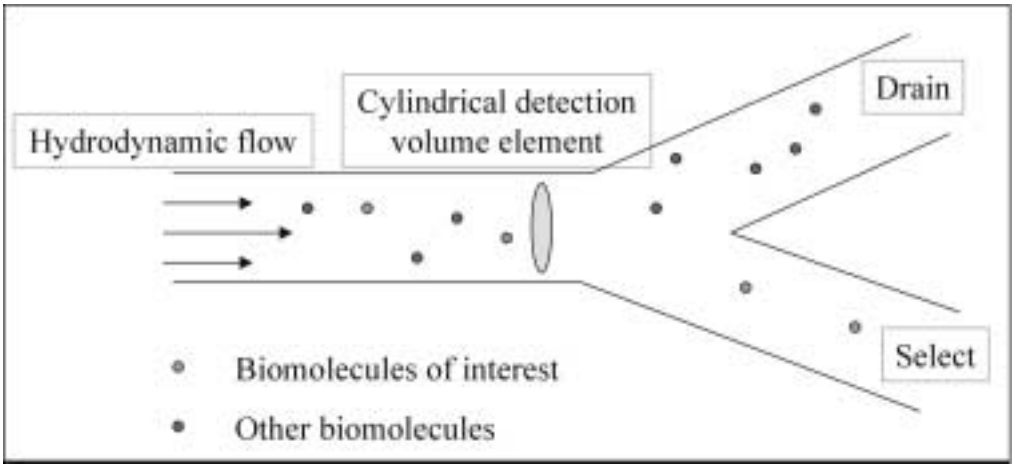

Figure 20 Molecule selection principle.

Although single molecule enrichment has not been achieved yet, initial measurements and tests with regards to the switching performance of an electrically driven high-speed micro dispensing valves (VHS) were performed. The valve is capable of performing switches on the millisecond range and therefore permits fractionating of, for instance, single biomolecules of biological libraries in fast flowing (> 5 mm/s)

pressure driven sample streams. To assemble a functional flow-switching device, a single valve was connected close to the 3-legged Y-shaped microstructure; the microstructure was fixed in a self-manufactured Plexiglas holder with polyethylene tubing connections (∅ 0.18 mm). The loading and hydrodynamic flow in the microstructures was achieved with a 250-µL syringe in a syringe pump connected with the microstructure via tubing. A flow velocity of 0.6 µl/min (corresponding to 5 mm/s) was applied to a liquid having 3 µm silica beads flowing from the 'inlet'-channel to the 'drain'-channel. The VHS-valve was actuated once per second for a duration of 3 ms. This had the effect of directing below 50 pl samples of fractionated bead sample, containing ensembles of beads, into the 'select' channel of the microstructure. As one can see in Figure 21, each time the VHS-valve was actuated a population of beads was fractionated. Fractionation was visualized with a CCD camera.

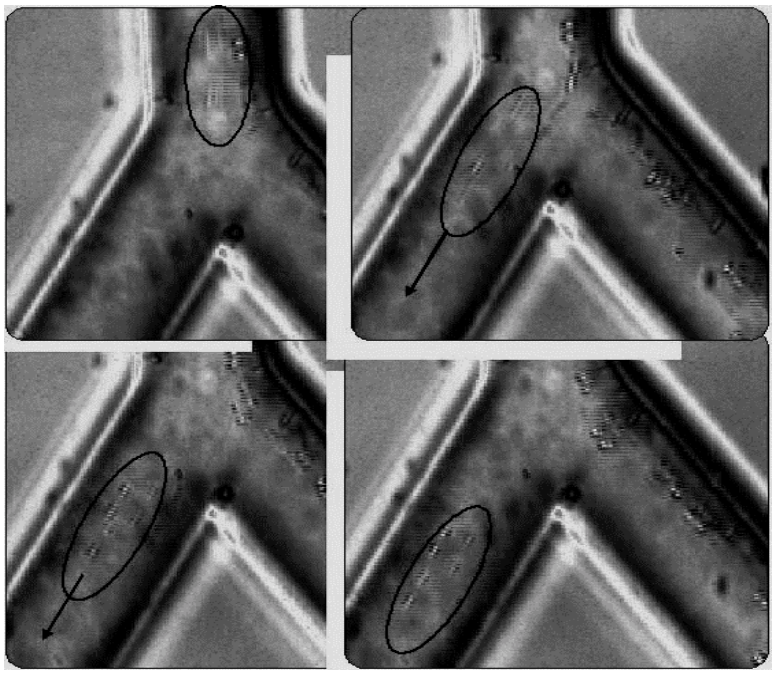

Figure 21 Realization of flow switching in a 50 x 50 µm^2 channel. It can be seen that a small ensemble fraction of beads (∅ 3 µm) is fractionated into the left channel. The fractionated volume was estimated to be 50 – 100 pl.

6.3. Conclusions – Single Molecule Detection in Flow

Single molecule detection in commercially available silicon-glass microfluidic structures has been performed. Cw laser light excitation enabled us to detect molecules with an average S/N of 4 at a flow velocity of 10 mm/s and a S/N of 7 at 5 mm/s in silicon glass microstructures. However, even though not all molecules of interest

might be detected and the detection probability is low (which is of importance for some single molecule analytical methods), these values are still sufficient to increase the throughput. In addition, a better detection efficiency can be obtained by decreasing the background with other window materials (e.g. PMMA or quartz glass structures). For biomolecular applications such as molecular selection or screening, the attachment of more than one dye onto the molecule of interest would increase the signal too. However, the labeling is not trivial because an increase in the number of dyes per molecule in the sample does not necessarily mean that the count rate per molecule increases linearly, since quenching[172] can occur. Moreover, utilizing a pulsed diode could decrease the scattering and Raman scattering light contribution further. The fluorescent lifetime of molecules, which can be determined for individual molecules by fluorescent burst analysis, is in the region of 1 – 10 ns and thereby well separated from the Raman scattering contribution which is in the sub-ns time range.

Bigger detection volume elements, as is shown for the elliptical excitation volume element, are difficult to use, since the background constribution increases dramatically with the volume size. If many molecules have to be detected or to be screened, a bigger detection volume element in combination with a flow cell can be advantageous when the fluorescent count rate of the molecules of interest is sufficiently high, because the throughput is increased. The Alzheimer's Aβ-peptide aggregates are a good example for highly fluorescent particles. Theses aggregates give a sufficiently high fluorescent signal that can be discriminated against the background even with an elliptical line focus set-up. Since relative differences in aggregate number might already reveal the state of health of a patient, a simple counting of fluorescent bursts with a certain threshold could be sufficient. In this case, for example, more than a fixed amount of Aβ-peptide aggregates would be an identification of Alzheimer's disease.

For the up-concentration of biomolecular or chemical libraries, microfluidics were investigated. It turned out that pl switching in the millisecond range is possible. However, since libraries with highly fluorescent biomolecules of interest have not been developed yet, the feasibility of such a single molecule selection machine will remain to be shown with selection experiments made on small silica or polystyrene beads that can be highly loaded with fluorescent dyes.

7. DNA-degradation on the Single Molecule Level (paper VIII)

Within recent decades, DNA sequencing has become a widely used tool in genetics, clinical applications, and diagnostics. In the late 70s, Frederic Sanger and co-workers[173] invented a DNA sequencing method based on amplification and electrophoretic separation of statiscitcally terminated fragments. The sequencing machines used today utilize this technique, which has been greatly improved in the last decades. Due to parallelization and automation the whole analysis process has been accelerated by some orders of magnitude. The method itself, however, is limited to sequences of only about 1000 – 2000 bp long fragments per experiment, due to the resolution of the gel. Researchers wanting to sequence longer fragments, for instance, a whole gene containing around 100 000 base pairs, have to sequence overlapping fragments of the gene. After identifying the bases, complex computer programs have to be used to deduce the right order of the pieces. These steps are time consuming and, for instance, replication errors, induced by PCR amplification of the target, are amplified as well.[121] Therefore, single molecule DNA sequencing has been proposed by Keller and coworkers[1] as an alternative. Using this method, DNA segments as long as 100 000 bp could be sequenced without amplification. This would simplify and speed up the sequencing task, since no computational reconstruction of bp-fragments to the DNA sequence would be needed. The proposed method is based on fluorescence detection and identification of cleaved, single dye labeled nucleotides as they are carried downstream through a detection volume element by flow.[2,42,50,51,142,144,145,174,175] In the detection area, the dyes announce their presence with a light flash. The detection rate or sequencing velocity is determined by the cleavage rate of the exonuclease enzyme sequentially cutting the nucleotides from the DNA. In this sequencing method, the DNA is usually attached to beads, which are held by either a capillary in a cytometry cuvette[1,50,51,53,59] or a laser pipette in capillaries or microstructures.[19,56,176,177] Other approaches using DNA attached to microloaders (fiber) inside of femto-tips have been investigated by Sauer *et al*.[58] In all experiments flow has been induced by either pressure or electroosmosis forces. In order to distinguish the four different bases by their fluorescent properties, different detection techniques like burst rates,[24] emission wavelengths,[56] lifetime determinations,[2,6,10,14,102,178,179] or a combination of these can be uesd.[18] A special issue; 'DNA-Sequencing at the Single Molecule Level' is dedicated and published in the Journal of Biotechnology with Rigler and Seela as guest editors.

7.1. The Single Molecule Sequencing Method

In our DNA degradation method introduced here (Figure 22, left), a dye-labeled DNA strand (produced by primer extension from a 5'-biotin labeled primer) was attached to a 1 µm streptavidine coated silica bead. The DNA loaded beads were inserted into the sample inlet channel of a 4-leg microstructure (Figure 22, right). With an infrared diode pumped Nd:YAG laser (CrystaLaser, IRCL-1.5W-1064), the beads were trapped in the sample zone. This so called 'optical tweezer'[180] enables to trap a bead in sample flows having for velocities up to several mm/s. After trapping one bead, the microstructure was moved and the bead thereby transported into the buffer channel. Here, the bead was cleaned from all non-specific bound dyes for approximately one minute. Next, the microstructure was moved again in order to position the bead in the enzyme flow where DNA degradation started immediately. The cleaved labeled nucleotides were transported by pressure driven flow to the excitation volume of a pulsed diode laser (638 nm, 60 MHz, PicoQuant GmbH), which was located five to seven (dependent on the set-up) µms further downstream. With this pulsed detection laser, different dyes with similar absorption spectra can be detected and distinguished from each other by measuring the lifetime of the dye-labeled nucleotides. Here, up to three different dyes can be distinguished and determined with lifetime measurements resulting in a classification probability of less than 65 %. In addition, emission wavelength detection is needed if a classification probability of approximately 99 % is desired.[18] In order to sequence DNA with lifetime determinations only, the DNA has to be sequenced several times.

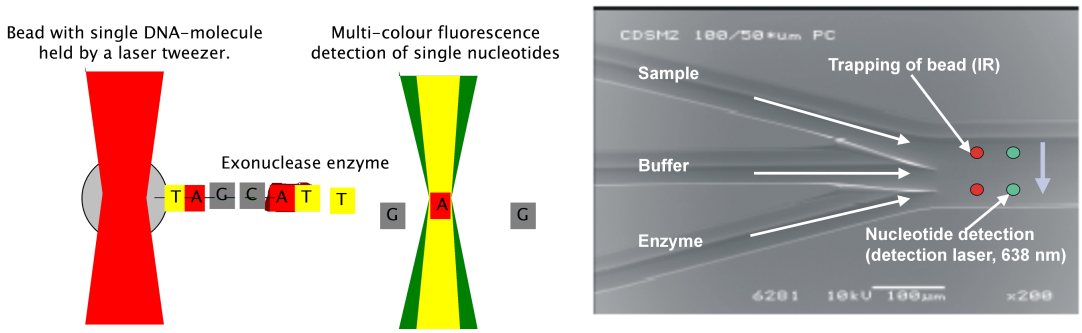

Figure 22 (left) The principle of single molecule DNA sequencing. (right) 4-leg microstructure with sample, buffer and enzyme inlet. Laminar fluidic zones are formed so that no mixing occurs in the broader exit channel.

7.2. Microstructures – Experimental

The background signal was kept low by using PMMA microstructures. The microchannels, 50 µm deep, and 50 and 150 µm wide, respectively, were patterned with injection moulding technology onto 1.4 mm thick PMMA plates and covered with a 170 µm PMMA lid. PMMA is a transparent material and exhibits low reflection (scattering) and autofluorescence for both the laser-diode excitation as well as the IR-trapping laser. Via-holes were drilled into the substrate at the end of the channels to enable a simple connection to the sample reservoir. In the PMMA microstructures a count rate of 30 kHz per Cy5-dUTP molecule was obtained, which was sufficient to detect single molecules in flow and to determine the enzymatic reaction on the bead bound DNA.

The microstructure was fixed in a self-made holder, which was connected to syringes via Teflon tubes (having inner core diameters of 170 µm). All liquid guiding parts (tubes, ferrules and O-rings) were disposable to avoid contamination. The holder was placed on a x-y stage (Märzhäuser) to align the structure with respect to the laser foci. Pressure driven flow and degassed buffer were used to avoid problems like clogging and air bubbles. In addition, the inlet channels merge into an exit channel having three times the width of the inlet channel, which enables resistance-free and stable flow. With this microstructure and the appropriate flow set-up, degradation measurements were achieved reproducible.

7.3. Target Principle (TP) – Experimental

In order to detect all the labeled nucleotides released from the bead, some detailed investigations regarding the positioning of the bead with respect to the detection volume element were made. To address this difficulty, the expression Target Principle (TP) has been introduced. The idea of the TP is that despite the presence of diffusion, all cleaved nucleotides pass through the detection volume. The correct combination of the bead position with respect to the detection volume element, the size of the detection volume, the distance between the detection volume and the bead, the flow speed, and the viscosity of the enzyme solution was thereby of importance. In the following, these considerations were taken into account and some experiments will show how the TP was realized in our set-up.

7.3.1. Alignment of the Bead with respect to the Detection Volume Element

In the DNA degradation set-up two different wavelengths (638 and 1064 nm) must be aligned with respect to each other in three-dimensional space. Since simple Gaussian optics predicts that any laser waist is focused at the focal distance, dependent on the wavelength, λ, $\left(s = f/1+\left(\lambda f/\pi\omega_0^2\right)^2\right)$, variations between the IR-focus and the HeNe-focus are pre-determined. This holds true even though the objective in use has already been corrected for chromatic aberrations. In addition, the beams entering the microscope objective might not be optimally collimated, which would in turn change the focal plane, too. Due to the differences in height observed for the two lasers and the fact that the bead is usually not trapped in the middle of the focus but slightly above,[180] other experiments were conducted and positioning techniques had to be found to assure the correct position of the trapped bead with respect to the detection laser focus.

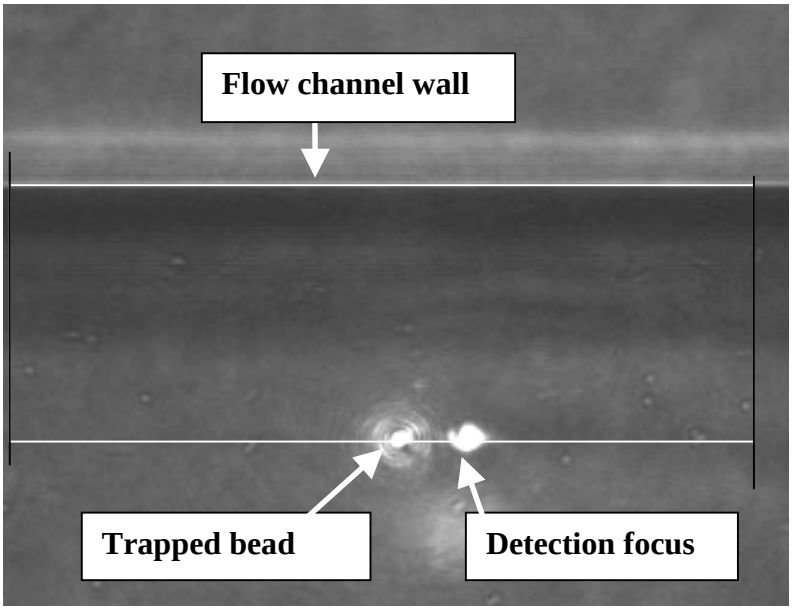

Figure 23 Visual alignment of the trapped bead with respect to the detection focus parallel to the flow direction.

The IR-focus position was aligned with respect to the detection focus through adjustments of a Gimbal-mounted mirror and also through adjustments of the distance between the two lenses in the beam expander. A magnified image of the trapped bead in the microchannel and framing software have been used to align the bead and the detection focus with respect to each other in the direction of the flow (Figure 23). The bead was considered to be aligned, when its position coincided with that of

the detection laser on the lower edge of the frame, the frame having been aligned with respect to the microchannel wall beforehand. Then, the optimal height-position on the optical axis was found by looking at the reflection of the detection laser of a naked bead when both foci coincided in all directions. The bead was scanned in the direction of the laser beam through the diode laser detection focus by moving one of the collimator lenses in the z-direction (Figure 24). Thereby, different reflection intensities were observed. The intensity was recorded as a function of the height-position (z-position) of the IR-laser beam relative to that of the trapped bead. After scanning in the z-direction in this manner, the IR-laser beam together with the bead was adjusted back to the z-position which had yielded the maximum scattered intensity; this was found within ± 0.5 µm. Finally, the IR-trapping laser was moved upstream away from the detection laser focus in the direction of flow, and finally, the alignment was confirmed by measuring the release of dyes from a heavily doped bead. We had difficulties to quantify the precision of this alignment method, since apart from the visual inspection, no alternative quantification tool was found. However, we estimated the physical alignment of the bead with respect to the detection focus having an absolute precision of ± 250 nm in both the direction perpendicular and parallel to the flow. Positioning to fix the distance between the trapped bead and the detection volume element was estimated to be precise to within ± 500 nm.

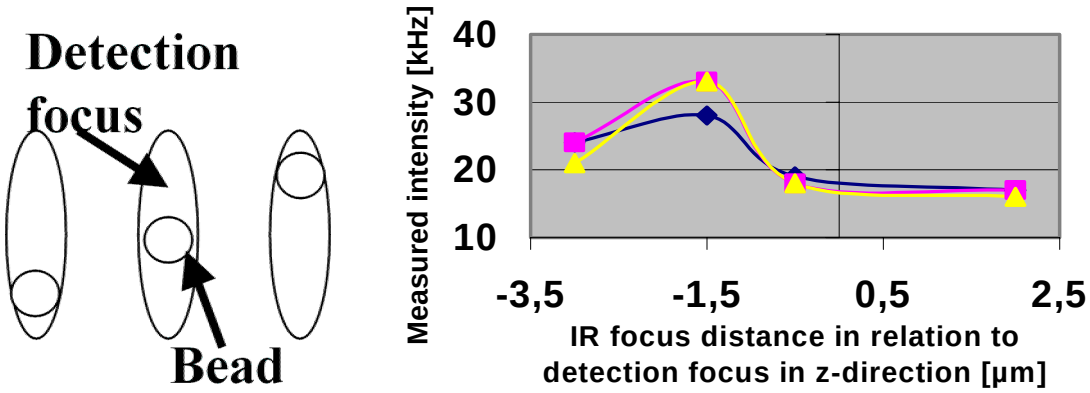

Figure 24 (left) Position of trapped bead scanned through detection focus. (right) Relative IR-scan range –3 to 2 µm (in the z-direction). Spline-fits of experimentally measured data.

7.3.2. Flow Simulations – Diffusion Effect on Flow Transported Molecules

Diffusion simulations for different flow velocities were made to find the optimal size of the detection volume element and the optimal buffer viscosity. A simulation example is displayed in Figure 25 and Figure 26 (Figure 26 is a magnification of the first 7-8 µm downstream from the bead in the direction of flow). Here, two liquids with the

same viscosity, separated by a thin wall and flowing from left to right parallel to each other were assumed. At a certain point the wall ended and the lateral displacement of molecules with a given diffusion constant (D = 190 µm^2/s in pure water) was simulated for a transport distance of 50 µm at a given flow velocity. The point where the wall ended corresponded to the position of the bead center.

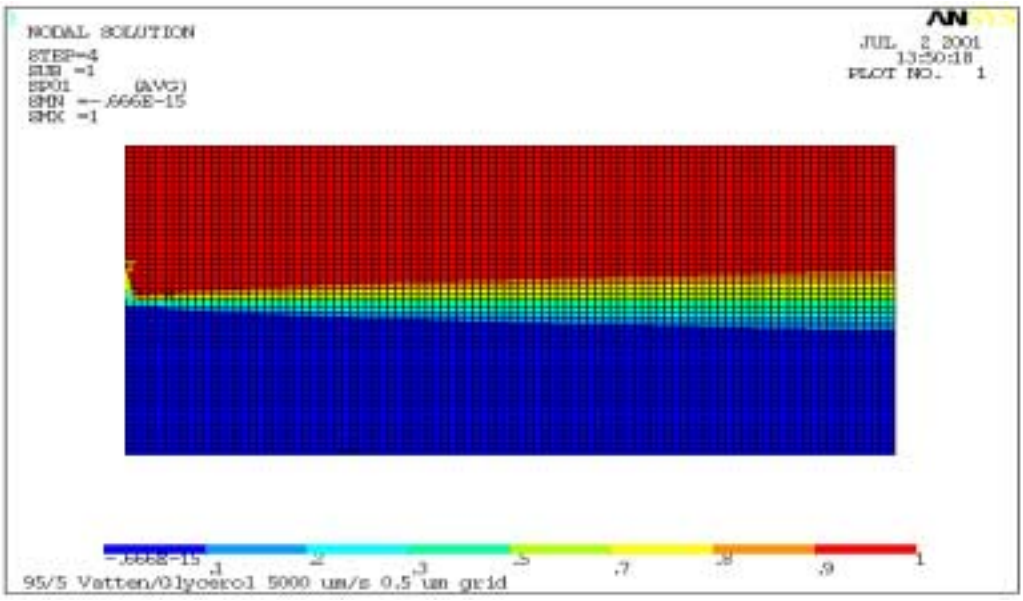

Figure 25 Simulation of two liquids that (both) contain 95 % water and 5 % glycerol; D for the molecules of interest in these conditions 190.5 µm^2/s. The flow velocity is 5 mm/s, and the element size in the grid is 0.5 µm^2.

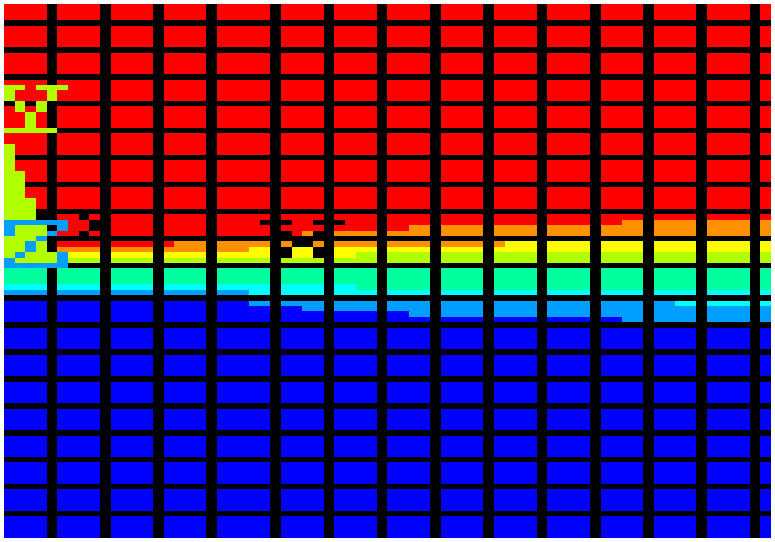

Figure 26 Enlargement of Figure 25. The figure is slightly more than 14 elements long (7 µm). At the far right, the diffusion cone is 2 µm high (4 elements). At the border between the darkest and the next darkest region there is a 90/10 % mixture of the diffusing molecules of the two liquids.

From the simulations we could project that with a detection volume element of 2 μm radial diameter (and a 4 – 6 μm depth for a Gaussian excitation beam), positioned 7 μm further downstream from the detection volume element in a 95/5 % mixture of water/glycerol with a flow speed of 5 mm/s, it is possible to detect 90 % of the molecules released from the bead. In order to confirm this projection, cross-correlation measurements on fluorescent molecules in a sample stream with DOE-generated diffraction limited foci were performed confirming the theoretically simulated values (see also chapter 2). Therefore, the theoretically determined flow speeds and detection volume element size values were used for the degradation experiments described later in this section. Additionally, since this flow is very slow and the Reynolds number well below 1 ($R = V\,l\rho/\eta$ = *0.006,* whereby V is the flow velocity, l the length of the fractional layer, ρ the fluid density and η the fluid viscosity), the laminar layers flowing towards the bead are a mirror image of the laminar layers flowing from the bead, which means in our case that molecules originating from the edge of the bead will be transported closer to the center of the flow axis (Figure 27). If this theory holds true, the detection efficiency will be further increased and it will appear in the detection volume that almost all molecules pass through the center of the bead.

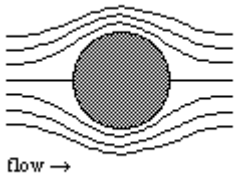

Figure 27 For slow velocities (Re < 1) the laminar layers of flow to the bead are a mirror image of flow from the bead.

A comment regarding the parameters has to be made, since theoretically numerous permutations of values for the five parameters (distance between the detection focus and the trapped bead, size of the bead, size of the detection focus, flow velocity, viscosity) would give a detection efficiency of 90% or more. We made simulations for flow velocities of 1, 3, 5, 7 and 10 mm/s, with water/glycerol mixtures of 100/0, 95/5, 90/10, 85/15, and 75/25 % (not shown). However, the values presented above were chosen due to some limitations. First, an increase in flow speed would give less stable bead trapping. The escape velocity, for the given power output of the IR-laser (approximately 600 mW), of a trapped bead used here is 12-16 mm/s in pure buffer flow. Second, a higher flow speed would result in the detection of fewer photons per labeled nucleotide per passage time making nucleotide classification difficult or even

impossible. Third, with a larger percentage of glycerol the refractive index value of the medium (n_b) gets closer to the refractive index of the bead (n) and since the gradient force only exceeds the scattering force and thereby holds the bead for $n > n_b$, the trapping force would be decreased. Fourth, for larger detection volume elements there is more detection laser light scattered from the walls of the microstructure and this could damage (e.g. photobleach) the bead-bound DNA. Therefore, only a detection volume smaller than 3 µm in radial diameter was used and the distance between the bead and the detection volume element was kept at 5-7 µm and could not be decreased. Finally, the bigger the bead the more difficult is it to keep the bead with the optical tweezer in the flow, since higher drag forces are present.

7.4. Enzymatic Degradation in Flow – Results

The silica beads were loaded with ssDNA (300 nt natural DNA), where in 80 % of all the natural thymine bases had been replaced by Evoblue-uracil. In hanging droplet experiments the number of DNA molecules per bead was calculated by adding exonuclease I, measuring the sample with FCS (not shown) and evaluating the obtained autocorrelation. In addition, the number of beads per sample volume was counted in a Bürker-chamber. With this information the number of fluorescent molecules per bead and thus the total number of ssDNA molecules per bead was determined. In the following, degradation experiments with about 100 DNA-strands per bead, thereby exhibiting approximately 6000 fluorescent dyes per bead, were performed. In order to extract more information from of the raw intensity trace, a ‘sliding window’ (moving average) method was applied. Here, a time frame with 200 µs width, corresponding to the passage time of molecules flowing at 5 mm/s through a 2 µm (radial diameter) detection volume element, was used fo a averaginig of the raw intensity trace in Figure 28 (left). Thereby, fluorescent bursts with a width corresponding to the passage time were detected and the maximum counts per molecule per passage time obtained. A burst was identified, when a predefined threshold (in this case 8 counts) was executed (corresponding to a S/N of 2–3). In Figure 28 (right), the burst frequency is determined, giving the number of bursts obtained per time unit. After displaying the obtained burst trace against the measurement time, different periods of the degradation experiment could be identified. At first, the DNA loaded bead was trapped in the sample channel and then transported into the buffer zone (P1, Figure 22). Here, it was held for one minute in order to wash free dyes from the bead. At P2 the bead was transported from the buffer channel into the enzyme channel. As can be seen, the enzymatic reaction took place immediately and

an increase in number of bursts per second was observed. During P3 the bead was held in the enzyme channel. Then in P4 the bead was released and the detection laser was kept in place in order to determine the background level in the enzyme channel. After that, again as a control measurement, the detection laser was moved into the buffer (washing) channel at P5 and the buffer background without the bead was recorded during P6. From the curve in Figure 28 (right) the degradation speed was determined. Two characteristic decay periods were identified: the washing step in phase P1, and the degradation step in phase P3. For the washing step approximately 500 nucleotides were detected over a period of 20 seconds, which means that approximately 25 nucleotides per second were washed away from the bead. This is a considerable amount and more careful measurements have to be made in order to see if the non-specific binding of the molecules can be avoided. In phase P3, 2000 nucleotides were released over a period of 20 seconds, corresponding to 100 molecules per second and an approximate detection efficiency of 33%. The reason for it lies mainly in the high background obtained of nonspecific bound dyes. However, neglecting the unspecific bound dyes to the bead, a cleavage rate of 1 nucleotide per second could be calculated for 80 % incorporated Evoblue-dUTP labeled natural DNA degraded with exonuclease Exo I.

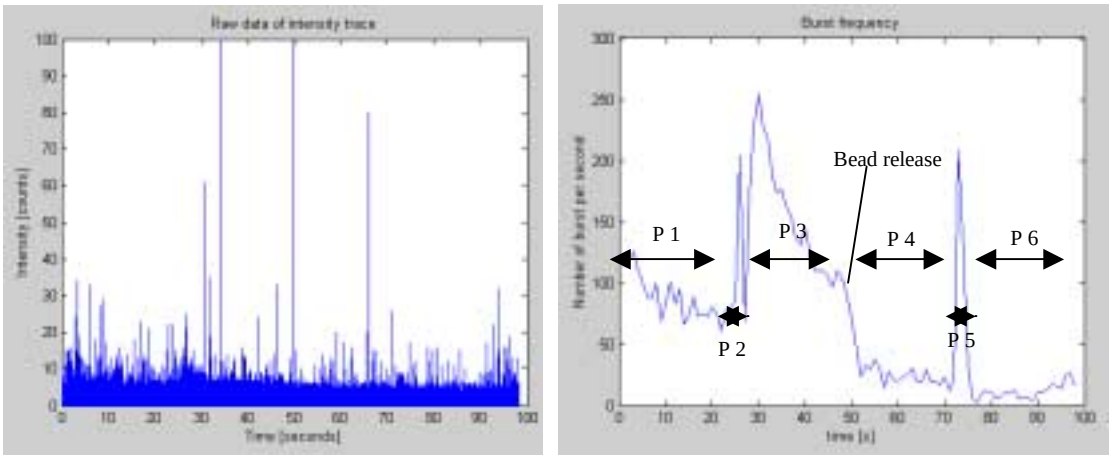

Figure 28 (left) Raw data of intensity trace. The bin size is 50 µs. (right) Burst frequency trace obtained with the 'sliding window' method. The bin size corresponds to the passage time of the molecules through the detection volume element and is 200 µs. The threshold (recognition rate) was 8 photons per bin (2σ), since the background average was 4 photons per bin.

7.5. Conclusions – DNA-degradation on the Single Molecule Level

Reproducible enzyme degradation measurements in microfluidic structures were performed. Single molecule bursts were identified, and expected intensity fluctuations in accordance to the movement of the trapped bead in the microstructure, were obtained that were comparable to degradation process described in literature.[145] The system shows full biochemical functionality and DNA with labelled nucleotides incorporated can be degraded by exonuclease in flow within microstructures. Also, the experiments show that the set-up features a stable fluidic system where beads and liquids can be handled and delivered reproducibly. Finally, the experiment shows the full functionality of the optical system: beads can be trapped and transported in a robust way, the optical alignment of the target system is good, and fluorophores can be detected and counted on the single molecule level. However, the system has to be improved with regard to photostability, quantum yield and S/N of the molecules in order to discriminate each cleaved molecule from the background. In addition, there is a need to identify and isolate enzymes which rapidly cleave nucleotides from non-natural DNA, in order to make this method competitive and advantageous to present PCR-based DNA sequencing methods.

8. Conclusions

The ultimate goal of performing parallel single molecule detection and analysis in biological samples in order to reach a higher throughput has been achieved. A novel multiple confocal foci excitation (DOE) and detection (CMOS-SPAD) concept has been utilized and integrated into a common fluorescence detection set-up. Analyte concentrations were determined and results thus obtained were comparable to those obtained using single confocal focus excitation and detection. Although some drawbacks such as low photon detection probability, especially in the red region, were present in the prototype and serve to prevent the total obsolescence of commercially available APDs, the first total integrated parallel single molecule detection instrumentation has been shown to be feasible. The potential for on-chip processing and data analysis integration makes this CMOS-detector array especially preferable to commercially available APDs. In addition to that, dual-color multi-focal cross-correlation analysis was performed. Here, new possibilities to detect single molecules at ultra-low concentrations by increasing the fluorescent even rate of the cross-correlating sample were found.

In addition, single molecule detection and thereby low-concentration analysis in microfluidic structures with the objective to increase the throughput has been shown. This method paves the way for a variety of applications where analysis and control measurements of low quantities are needed. The advantage of combining microstructures together with this ultra sensitive detection method is that, in addition to the low concentration a small amount of sample liquid is used. Furthermore, it has been shown that FCS can be used to characterize and monitor flow with sub-µm precision. The great advantage of diffraction limited detection has thereby been utilized.

Finally, a system for reproducible DNA degradation measurements has been designed and experiments were performed. For this purpose, a well functioning fluidic system, stable bead trapping, and a fully functioning target principle had to be established. The 4-leg microstructure used allowed for stable and laminar flow zones, with excellent separation of sample and enzyme. The DNA loaded beads could be transported by optical tweezers across the hydrodynamic flow profile of the microfluidic channel, without loss of control. The alignment precision of the bead with respect to the detection volume element was less than $\pm$ 250 nm. In addition, theoretical simulations and experiments showed that a detection probability of approximately 90 % could be achieved.

9. Outlook

The motivation for faster analysis, higher sample throughput, and smaller sample consumption is well known and drives instrument development towards integrated and multi-tasking detection systems. The beauty of single molecule analysis is that on a molecular level it represents analysis of the smallest entity. On the other hand the drawback with it is that one must analyze the smallest possible entity if to obtain an advantage. Therefore, the interface between the detection of single molecules and the macroscopic world, where, for example, the biology still works in µl-units in order to make bio-chemical reactions work, is of great importance and has to be navigated so that an unhindered transfer between these two worlds is possible and 'real' single molecule applications become feasible.

The parallel confocal detection technique described is only one piece of the analysis puzzle. In order to have a total integrated analysis system, sample handling and data processing have to be included too. The use of microfluidic systems represents one step forward already. Still exceedingly large quantities (a couple of µl of sample) are used during these experiments. More effort has to be placed on the continued development of microarrays, since the minimal sample amount that can be used in commercial instruments is still seldom below 1 µl and the concentrations involved are mostly still in the nanomolar regime (e.g. ~10^{12} molecules per µl). In addition, even though data processing is in 'high throughput drug validation streets' automated, still a surfeit of data is obtained and has to be analyzed to extract the information one would like to retrieve. The best example, wherein 'real' single molecule application ought to become feasible is the single molecule degradation of DNA. If it would be possible to attach one DNA strand on as few as 10 beads and to analyze them with a high detection efficiency (> 90 %), a real advantage would be obtained and this would represent a revolutionary step forward in the area of biotechnology and life science.

In order to make 'real' single molecule analyses feasible within a couple of decades, a lot of effort must be placed on the total integration of high throughput systems including sample, microstructure, data analysis, and, last but not least incorporation of sound biology and chemistry precepts. Working with single molecules is of evident advantage since all other methods rely on PCR amplification, which exhibit an inherent problem of statistical averaging and error multiplication for each amplification step.

Bibliography

(1) Jett, J. H., Keller, R. A., Martin, J. C., Marrone, B. L., Moyzis, R. K., Ratliff, R. L., Seitzinger, N. K., Shera, E. B. and Stewart, C. C. "High-speed DNA sequencing: an approach based upon fluorescence detection of single molecules." (1989) *Journal of Bimolecular Structure and Dynamics*, **7**, p. 301-309.

(2) Soper, S. A., Keller, R. A., Shera, E. B., Martin, J. C. and Jett, J. H. "Single Molecule Detection of Fluorophores in Flowing Sample Streams Utilizing CW and Pulsed-Laser Excitation." (1990) *Abstracts of Papers of the American Chemical Society*, **200**, p. 135-ANYL.

(3) Shera, E. B., Seitzinger, N. K., Davis, L. M., Keller, R. A. and Soper, S. A. "Detection of Single Fluorescent Molecules." (1990) *Chemical Physics Letters*, **174** *(6)*, p. 553-557.

(4) Rigler, R. and Mets, Ü. "Diffusion of single molecules through a Gaussian laser beam." (1992) *SPIE*, **1921**, p. 553-557.

(5) Mets, Ü. and Rigler, R. "Submillisecond Detection of Single Rhodamine Molecules in Water." (1992) *Journal of Fluorescence*, **4** *(3)*, p. 259-263.

(6) Wilkerson, C. W., Goodwin, P. M., Ambrose, W. P., Martin, J. C. and Keller, R. A. "Detection and Lifetime Measurement of Single Molecules in Flowing Sample Streams by Laser-Induced Fluorescence." (1993) *Applied Physics Letters*, **62** *(17)*, p. 2030-2032.

(7) Trautman, J. K., Macklin, J. J., Brus, L. E. and Betzig, E. "Near-Field spectroscopy of single molecules at room temperature." (1994) *Nature*, **369**, p. 40-42.

(8) Ambrose, W. P., Goodwin, P. M., Martin, J. C. and Keller, R. A. "Single-Molecule Detection and Photochemistry on a Surface Using near-Field Optical-Excitation." (1994) *Physical Review Letters*, **72** *(1)*, p. 160-163.

(9) Nie, S. M., Chiu, D. T. and Zare, R. N. "Probing Individual Molecules with Confocal Fluorescence Microscopy." (1994) *Science*, **266** *(5187)*, p. 1018-1021.

(10) Tellinghuisen, J., Goodwin, P. M., Ambrose, W. P., Martin, J. C. and Keller, R. A. "Analysis of Fluorescence Lifetime Data for Single Rhodamine Molecules in Flowing Sample Streams." (1994) *Analytical Chemistry*, **66** *(1)*, p. 64-72.

(11) Eigen, M. and Rigler, R. "Sorting Single Molecules - Application to Diagnostics and Evolutionary Biotechnology." (1994) *Proceedings of the National Academy of Sciences of the United States of America*, **91** *(13)*, p. 5740-5747.

(12) Sauer, M., Drexhage, K. H., Zander, C. and Wolfrum, J. "Diode laser based detection of single molecules in solutions." (1996) *Chemical Physics Letters*, **254** *(3-4)*, p. 223-228.

(13) Zander, C., Sauer, M., Drexhage, K. H., Ko, D. S., Schulz, A., Wolfrum, J., Brand, L., Eggeling, C. and Seidel, C. A. M. "Detection and characterization of single molecules in aqueous solution." (1996) *Applied Physics B-Lasers and Optics*, **63** *(5)*, p. 517-523.

(14) Muller, R., Zander, C., Sauer, M., Deimel, M., Ko, D. S., Siebert, S., ArdenJacob, J., Deltau, G., Marx, N. J., Drexhage, K. H. and Wolfrum, J. "Time-resolved identification of single molecules in solution with a pulsed

semiconductor diode laser." (1996) *Chemical Physics Letters*, **262** *(6)*, p. 716-722.

(15) Machara, N. P., Goodwin, P. M., Enderlein, J., Semin, D. J. and Keller, R. A. "Efficient detection of single molecules eluting off an optically trapped microsphere." (1998) *Bioimaging*, **6** *(1)*, p. 33-42.

(16) Becker, W., Hickl, H., Zander, C., Drexhage, K. H., Sauer, M., Siebert, S. and Wolfrum, J. "Time-resolved detection and identification of single analyte molecules in microcapillaries by time-correlated single-photon counting (TCSPC)." (1999) *Review of Scientific Instruments*, **70** *(3)*, p. 1835-1841.

(17) Weiss, S. "Fluorescence spectroscopy of single biomolecules." (1999) *Science*, **283**, p. 1676-1683.

(18) Herten, D. P., Tinnefeld, P. and Sauer, M. H. M. "Identification of single fluorescently labelled mononucleotide molecules in solution by spectrally resolved time-correlated single-photon counting." (2000) *Applied Physics B*, **71**, p. 765-771.

(19) Stephan, J., Dörre, K., Brakmann, S., Winkler, T., Wetzel, T., Lapczyna, M., Stuke, M., Angerer, B., Ankenbauer, W., Földes-Papp, Z., Rigler, R. and Eigen, M. "Towards a general procedure for sequencing single DNA molecules." (2001) *Journal of Biotechnology*, **86**, p. 255-267.

(20) Rigler, R. and Elson, E. S., Eds. *Fluorescence Correlation Spectroscopy, Theory and Applications*; Springer- Verlag: Berlin Heidelberg New York, 2001.

(21) Krichevsky, O. and Bonnet, G. "Fluorescence correlation spectroscopy: the technique and its applications." (2002) *Reports on Progress in Physics*, **65** *(2)*, p. 251-297.

(22) Soper, S. A., Mattingly, Q. L. and Vegunta, P. "Photon Burst Detection of Single near-Infrared Fluorescent Molecules." (1993) *Analytical Chemistry*, **65** *(6)*, p. 740-747.

(23) Enderlein, J., Robbins, D. L., Ambrose, W. P. and Keller, R. A. "Molecular shot noise, burst size distribution, and single- molecule detection in fluid flow: Effects of multiple occupancy." (1998) *Journal of Physical Chemistry A*, **102** *(30)*, p. 6089-6094.

(24) Van Orden, A., Machara, N. P., Goodwin, P. M. and Keller, R. A. "Single molecule identification in flowing sample streams by fluorescence burst size and intraburst fluorescence decay rate." (1998) *Analytical Chemistry*, **70** *(7)*, p. 1444-1451.

(25) Bark, N., Rigler, R., Terenius, L. and Tjernberg, L. "Fluorescence burst analysis of cerebrospinal fluid as a diagnostic tool for Alzheimer's disease." (2002) *Neurobiology of Aging*, **23** *(1)*, p. 1382.

(26) Beebe, D. J., Mensing, G. A. and Walker, G. M. "Physics and applications of microfluidics in biology." (2002) *Annual Review of Biomedical Engineering*, **4**, p. 261-286.

(27) Taghizadeh, M. R., Blair, P., Layet, B., Barton, I. M., Waddie, A. J. and Ross, N. "Design and fabrication of diffractive optical elements." (1997) *Microelectronic Engineering*, **34** *(3-4)*, p. 219-242.

(28) Johansson, M., "Application and Design, Developments in Diffractive Optics" Doctoral Thesis, Chalmers University of Technology, Göteborg, Sweden, 2001.

(29) Rochas, A., Pauchard, A. R., Besse, P. A., Pantic, D., Prijic, Z. and Popovic, R. S. "Low-noise silicon avalanche photodiodes fabricated in conventional

CMOS technology." (2002) *IEEE Transactions on Electron Devices*, **49** *(3)*, p. 387-394.

(30) Santiago, J. G., Wereley, S. T., Meinhart, C. D., Beebe, D. J. and Adrian, R. J. "A particle image velocimetry system for microfluidics." (1998) *Experiments in Fluids*, **25** *(4)*, p. 316-319.

(31) Kopp, M. U., de Mello, A. J. and Manz, A. "Chemical amplification: Continuous-flow PCR on a chip." (1998) *Science*, **280** *(5366)*, p. 1046-1048.

(32) Hadd, A. G., Jacobson, S. C. and Ramsey, J. M. "Microfluidic assays of acetylcholinesterase inhibitors." (1999) *Analytical Chemistry*, **71** *(22)*, p. 5206-5212.

(33) Wabuyele, M. B., Ford, S. M., Barrow, J. and Soper, S. A. "Single Molecule Detection of Double-stranded DNA in poly (methylmethacrylate) and polycarbonate microfluidic devices." (2001) *Electrophoresis*, **22**, p. 3939-3948.

(34) Lenne, P. F., Colombo, D., Giovannini, H. and Rigneault, H. "Flow profiles and directionality in microcapillaries measured by fluorescence correlation spectroscopy." (2002) *Single Molecules*, **3** *(4)*, p. 194-200.

(35) Shelby, J. P. and Chiu, D. T. "Mapping fast flows over micrometer-length scales using flow- tagging velocimetry and single-molecule detection." (2003) *Analytical Chemistry*, **75** *(6)*, p. 1387-1392.

(36) Kask, P., Gunther, R. and Axhausen, P. "Statistical accuracy in fluorescence fluctuation experiments." (1997) *European Biophysics Journal*, **25** *(3)*, p. 163-169.

(37) Qian, H. "On the Statistics of Fluorescence Correlation Spectroscopy." (1990) *Biophysical Chemistry*, **38** *(1-2)*, p. 49-57.

(38) Li, L. Q. and Davis, L. M. "Single-Photon Avalanche-Diode for Single-Molecule Detection." (1993) *Review of Scientific Instruments*, **64** *(6)*, p. 1524-1529.

(39) Kindt, W. J. and Zeijl, H. W. "Modeling and fabrication of Geiger mode avalanche photodiodes." (1998) *IEEE Transactions on Electron Devices*, **45** *(3)*, p. 715-719.

(40) Moloney, A. M., Morrison, A. P., Jackson, J. C., Mathewson, A., Alderman, A., Donnelly, J., O'Neill, B., Kelleher, A. M., Healy, G. and Murphy, P. J. "Monolithically integrated avalanche photodiode and transimpedance amplifier in a hybrid bulk/SOI CMOS process." (2003) *Electronics Letters*, **39** *(4)*, p. 391-392.

(41) Jackson, J. C., Phelan, D., Morrison, A. P., Redfern, R. M. and Mathewson, A. "Toward integrated single-photon-counting microarrays." (2003) *Optical Engineering*, **42** *(1)*, p. 112-118.

(42) Eigen, M. and Rigler, R. "Sorting Single Molecules - Application to Diagnostics and Evolutionary Biotechnology." (1994) *Proc. Natl. Acad. Sci. U.S.A.*, **91** *(13)*, p. 5740-5747.

(43) Schwille, P., MeyerAlmes, F. J. and Rigler, R. "Dual-color fluorescence cross-correlation spectroscopy for multicomponent diffusional analysis in solution." (1997) *Biophysical Journal*, **72** *(4)*, p. 1878-1886.

(44) Rigler, R., Foldes-Papp, Z., Meyer-Alme, F. J., Sammet, C., Volcker, M. and Schnetz, A. "Fluorescence cross-correlation: A new concept for polymerase chain reaction." (1998) *Journal of Biotechnology*, **63** *(2)*, p. 97-109.

(45) Amediek, A., Haustein, E., Scherfeld, D. and Schwille, P. "Scanning dual-color cross-correlation analysis for dynamic co- localization studies of immobile molecules." (2002) *Single Molecules*, **3** *(4)*, p. 201-210.
(46) Bacia, K., Majoul, I. V. and Schwille, P. "Probing the endocytic pathway in live cells using dual-color fluorescence cross-correlation analysis." (2002) *Biophysical Journal*, **83** *(2)*, p. 1184-1193.
(47) Medina, M. A. and Schwille, P. "Fluorescence correlation spectroscopy for the detection and study of single molecules in Biology." (2002) *Bioessays*, **24** *(8)*, p. 758-764.
(48) Rarbach, M., Kettling, U., Koltermann, A. and Eigen, M. "Dual-color fluorescence cross-correlation spectroscopy for monitoring the kinetics of enzyme-catalyzed reactions." (2001) *Methods*, **24** *(2)*, p. 104-116.
(49) Jett, J. H., Keller, R. A., Martin, J. C., Seitzinger, N. K. and Shera, E. B. "Single Molecule Detection in Flowing Sample Streams as an Approach to DNA Sequencing." (1989) *Abstracts of Papers of the American Chemical Society*, **198**, p. 41-ANYL.
(50) Davis, L. M., Fairfield, F. R., Harger, C. A., Jett, J. H., Keller, R. A., Hahn, J. H., Krakowski, L. A., Marrone, B. L., Martin, J. C., Nutter, H. L., Ratliff, R. L., Shera, E. B., Simpson, D. J. and Soper, S. A. "Rapid DNA Sequencing Based Upon Single Molecule Detection." (1991) *Genetic Analysis-Biomolecular Engineering*, **8** *(1)*, p. 1-7.
(51) Ambrose, W. P., Goodwin, P. M., Jett, J. H., Johnson, M. E., Martin, J. C., Marrone, B. L., Schecker, J. A., Wilkerson, C. W., Keller, R. A., Haces, A., Shih, P. J. and Harding, J. D. "Application of Single-Molecule Detection to DNA-Sequencing and Sizing." (1993) *Berichte Der Bunsen-Gesellschaft-Physical Chemistry Chemical Physics*, **97** *(12)*, p. 1535-1542.
(52) Keller, R. A. "Applications of Single-Molecule Detection to DNA-Sequencing and Sizing." (1993) *Abstracts of Papers of the American Chemical Society*, **206**, p. 79-ANYL.
(53) Goodwin, P. M., Affleck, R. L., Ambrose, W. P., Demas, J. N., Jett, J. H., Martin, J. C., Reha-Krantz, L. J., Semin, D. J., Schecker, J. A., Wu, M. and Keller, R. A. "Progress towards DNA sequencing at the single molecule level." (1995) *Experimental Techniques in Physics*, **41**, p. 279-294.
(54) Schecker, J. A., Goodwin, P. M., Affleck, R. L., Wu, M., Martin, J. C., Jett, J. H. and Keller, R. A. "DNA sequencing via single molecule detection of enzymatically cleaved fluorescent nucleotides." (1995) *Proceedings in SPIE*, **2386**, p. 4-12.
(55) Goodwin, P. M., Cai, H., Jett, J. H., Keller, R. A. and Semin, D. J. "DNA sequencing by single molecule detection." (1996) *Progress in Biophysics & Molecular Biology*, **65**, p. SMI02-SMI02.
(56) Dörre, K., Brakmann, S., Brinkmeier, M., Han, K. T., Riebeseel, K., Schwille, P., Stephan, J., Wetzel, T., Lapczyna, M., Stuke, M., Bader, R., Hinz, M., Seliger, H., Holm, J., Eigen, M. and Rigler, R. "Techniques for single molecule sequencing." (1997) *Bioimaging*, **5**, p. 139-152.
(57) Werner, J. H., Cai, H., Goodwin, P. M. and Keller, R. A. "Current status of DNA sequencing by single molecule detection." (1999) *Proceeding in SPIE*, **3602**, p. 355-366.
(58) Sauer, M. H. M., Angerer, B., Ankenbauer, W., Földes-Papp, Z., Göbel, F., Han, K. T., Rigler, R., Schulz, A., Wolfrum, J. and Zander, C. "Single

Molecule DNA sequencing in submicrometer channels: state of the art and future prospects." (2001) *Journal of Biotechnology*, **86**, p. 181-201.

(59) Werner, J. H., Cai, H., Jett, J. H., Reha-Krantz, L., Keller, R. A. and Goodwin, P. M. "Progress towards single-molecule DNA sequencing: a one color demonstration." (2003) *Journal of Biotechnology*, **102** *(1)*, p. 1-14.

(60) Reyes, D. R., Iossifidis, D., Auroux, P. A. and Manz, A. "Micro total analysis systems. 1. Introduction, theory, and technology." (2002) *Analytical Chemistry*, **74** *(12)*, p. 2623-2636.

(61) Auroux, P. A., Iossifidis, D., Reyes, D. R. and Manz, A. "Micro total analysis systems. 2. Analytical standard operations and applications." (2002) *Analytical Chemistry*, **74** *(12)*, p. 2637-2652.

(62) Gerlach, A., Knebel, G., Guber, A. E., Heckele, M., Herrmann, D., Muslija, A. and Schaller, T. "Microfabrication of single-use plastic microfluidic devices for high-throughput screening and DNA analysis." (2002) *Microsystem Technologies*, **7** *(5-6)*, p. 265-268.

(63) Eyal, S. and Quake, S. R. "Velocity-independent microfluidic flow cytometry." (2002) *Electrophoresis*, **23** *(16)*, p. 2653-2657.

(64) Jackson, W. C., Bennett, T. A., Edwards, B. S., Prossnitz, E., Lopez, G. P. and Sklar, L. A. "Performance of in-line microfluidic mixers in laminar flow for high-throughput flow cytometry." (2002) *Biotechniques*, **33** *(1)*, p. 220-226.

(65) Park, T. H. and Shuler, M. L. "Integration of cell culture and microfabrication technology." (2003) *Biotechnology Progress*, **19** *(2)*, p. 243-253.

(66) Heo, J., Thomas, K. J., Seong, G. H. and Crooks, R. M. "A microfluidic bioreactor based on hydrogel-entrapped E. coli: Cell viability, lysis, and intracellular enzyme reactions." (2003) *Analytical Chemistry*, **75** *(1)*, p. 22-26.

(67) Harrison, D. J., Fluri, K., Seiler, K., Fan, Z. H., Effenhauser, C. S. and Manz, A. "Micromachining a Miniaturized Capillary Electrophoresis-Based Chemical-Analysis System on a Chip." (1993) *Science*, **261** *(5123)*, p. 895-897.

(68) Chang, H. T., Chen, H. S., Hsieh, M. M. and Tseng, W. L. "Electrophoretic separation of DNA in the presence of electroosmotic flow." (2000) *Reviews in Analytical Chemistry*, **19** *(1)*, p. 45-74.

(69) Yang, R. J., Fu, L. M. and Lin, Y. C. "Electroosmotic flow in microchannels." (2001) *Journal of Colloid and Interface Science*, **239** *(1)*, p. 98-105.

(70) Moorthy, J., Khoury, C., Moore, J. S. and Beebe, D. J. "Active control of electroosmotic flow in microchannels using light." (2001) *Sensors and Actuators B-Chemical*, **75** *(3)*, p. 223-229.

(71) Ghosal, S. "Effect of analyte adsorption on the electroosmotic flow in microfluidic channels." (2002) *Analytical Chemistry*, **74** *(4)*, p. 771-775.

(72) Chen, S. H., Lin, Y. H., Wang, L. Y., Lin, C. C. and Lee, G. B. "Flow-through sampling for electrophoresis-based microchips and their applications for protein analysis." (2002) *Analytical Chemistry*, **74** *(19)*, p. 5146-5153.

(73) Li, D. Q. "Electro-viscous effects on pressure-driven liquid flow in microchannels." (2001) *Colloids and Surfaces a-Physicochemical and Engineering Aspects*, **195** *(1-3)*, p. 35-57.

(74) Dutta, D. and Leighton, D. T. "Dispersion reduction in pressure driven flow through microetched channels." (2001) *Analytical Chemistry*, **73** *(3)*, p. 504-513.

(75) Rush, B. M., Dorfman, K. D., Brenner, H. and Kim, S. "Dispersion by pressure-driven flow in serpentine microfluidic channels." (2002) *Industrial & Engineering Chemistry Research*, **41** *(18)*, p. 4652-4662.

(76) Holden, M. A., Kumar, S., Beskok, A. and Cremer, P. S. "Microfluidic dillusion diluter: bulging of PDMS microchannels under pressure-driven flow." (2003) *Journal of Micromechanics and Microengineering*, **13** *(3)*, p. 412-418.

(77) Wang, X. J., Milner, T. E. and Nelson, J. S. "Characterization of Fluid-Flow Velocity by Optical Doppler Tomography." (1995) *Optics Letters*, **20** *(11)*, p. 1337-1339.

(78) Nitta, N., Hagihara, K. and Shiina, T. "Experimental investigation of 3-D blood flow velocity measurement." (1996) *Japanese Journal of Applied Physics Part 1-Regular Papers Short Notes & Review Papers*, **35** *(5B)*, p. 3126-3130.

(79) Chen, Z. P., Milner, T. E., Dave, D. and Nelson, J. S. "Optical Doppler tomographic imaging of fluid flow velocity in highly scattering media." (1997) *Optics Letters*, **22** *(1)*, p. 64-66.

(80) Ren, H. W., Chen, Z. P., Brecke, K. M., Ding, Z. H., Zhao, Y. H. and Nelson, J. S. "Imaging transverse flow velocity using spectral bandwidth of the Doppler frequency shift in phase-resolved optical Doppler tomography." (2002) *Lasers in Surgery and Medicine*, p. 297.

(81) Piao, D. Q., Otis, L. L. and Zhu, Q. "Doppler angle and flow velocity mapping by combined Doppler shift and Doppler bandwidth measurements in optical Doppler tomography." (2003) *Optics Letters*, **28** *(13)*, p. 1120-1122.

(82) Adrian, R. J. "Particle-Imaging Techniques for Experimental Fluid-Mechanics." (1991) *Annual Review of Fluid Mechanics*, **23**, p. 261-304.

(83) Manz, B., Stilbs, P., Jonsson, B., Soderman, O. and Callaghan, P. T. "NMR Imaging of the Time Evolution of Electroosmotic Flow in a Capillary." (1995) *Journal of Physical Chemistry*, **99** *(29)*, p. 11297-11301.

(84) Maynes, D. and Webb, A. R. "Velocity profile characterization in sub-millimeter diameter tubes using molecular tagging velocimetry." (2002) *Experiments in Fluids*, **32** *(1)*, p. 3-15.

(85) Paul, P. H., Garguilo, M. G. and Rakestraw, D. J. "Imaging of pressure- and electrokinetically driven flows through open capillaries." (1998) *Analytical Chemistry*, **70** *(13)*, p. 2459-2467.

(86) Lempert, W. R. and Harris, S. R. "Flow tagging velocimetry using caged dye photo-activated fluorophores." (2000) *Measurement Science & Technology*, **11** *(9)*, p. 1251-1258.

(87) Elson, E. L. and Magde, D. "Fluorescence Correlation Spectroscopy I: Conceptual Basis and Theory." (1974) *Biopolymers*, **13**, p. 1-27.

(88) Magde, D., Elson, E. and Webb, W. W. "Fluorescence correlation spectroscopy II: An experimental realization." (1974) *Biopolymers*, **4**, p. 29-61.

(89) Magde, D., Webb, W. W. and Elson, E. "Fluorescence Correlation Spectroscopy. III. Uniform Translation and Laminar Flow." (1978) *Biopolymers*, **17**, p. 361-376.

(90) Ehrenberg, M. and Rigler, R. "Rotational brownian motion and fluorescence intensity fluctuations." (1974) *Chemical Physics*, **4** *(3)*, p. 390-401.

(91) Aragón, S. R. and Pecora, R. "Fluorescence correlation spectroscopy as a probe of molecular dynamics." (1976) *Journal of Chemical Physics*, **64**, p. 1791-1803.
(92) Rigler, R., Mets, U., Widengren, J. and Kask, P. "Fluorescence Correlation Spectroscopy with High Count Rate and Low-Background - Analysis of Translational Diffusion." (1993) *European Biophysics Journal*, **22** *(3)*, p. 169-175.
(93) Marquardt, D. W. "An algorithm for least-squares estimation of non-linear parameters." (1963) *Journal of Science, Industrial Applications and Mathematics*, **11** *(2)*, p. 431-441.
(94) Bengtsson, J. "Design of fan-out kinoforms in the entire scalar diffraction regime wihth an optimal-rotation-angle method." (1997) *Applied Optics*, **36**, p. 8435-8444.
(95) Brinkmeier, M., Dorre, K., Stephan, J. and Eigen, M. "Two beam cross correlation: A method to characterize transport phenomena in micrometer-sized structures." (1999) *Analytical Chemistry*, **71** *(3)*, p. 609-616.
(96) Marton, M. J., DeRisi, J. L., Bennett, H. A., Iyer, V. R., Meyer, M. R., Roberts, R., Stoughton, J., Burchard, D., Slade, D., Dai, H., Bassett, D. E., Hartwell, L. H., Brown, P. O. and Friend, S. H. "Drug target validation and identification of secondary drug target effects using DNA microarrays." (1998) *Nature Med.*, **4**, p. 1293-1301.
(97) Holmberg, A. "DNA-microarrays: novel techniques to study aging and guide gerentologic medicine." (2000) *Experimental Gerentology*, **36**, p. 1189-1198.
(98) Lockhart, D. J. and Winzeler, E. A. "Genomics, gene expression and DNA arrays." (2000) *Nature*, **405**, p. 827-836.
(99) Lipshutz, R. J., Fodor, S. P. A., Gingeras, T. R. and Lockhart, D. J. "High density synthetic oligonucleotide arrays." (1999) *Nature Genetics*, **21**, p. 20-24.
(100) Blom, H., Johansson, M., Hedman, A. S., Lundberg, L., Hanning, A., Hard, S. and Rigler, R. "Parallel fluorescence detection of single biomolecules in microarrays by a diffractive-optical-designed 2 x 2 fan-out element." (2002) *Appl. Opt.*, **41** *(16)*, p. 3336-3342.
(101) Mehta, D. S., Lee, C. Y. and Chiou, A. "Multipoint parallel excitation and CCD-based imaging system for high-throughput fluorescence detection of biochip micro-arrays." (2001) *Optics Communications*, **190** *(1-6)*, p. 59-68.
(102) Hungerford, G. and Birch, D. J. S. "Single-photon timing detectors for fluorescence lifetime spectroscopy." (1996) *Measurement Science & Technology*, **7** *(2)*, p. 121-135.
(103) Muller, A., Gisin, N. and Pellaux, J. P. "Decay Time Measurement of Fluorescent Fibers with Photon- Counting." (1993) *Review of Scientific Instruments*, **64** *(5)*, p. 1158-1160.
(104) Wennmalm, S., Blom, H., Wallerman, L. and Rigler, R. "UV-fluorescence correlation spectroscopy of 2-aminopurine." (2001) *Biological Chemistry*, **382** *(3)*, p. 393-397.
(105) Spinelli, A., Davis, L. M. and Dautet, H. "Actively quenched single-photon avalanche diode for high repetition rate time-gated photon counting." (1996) *Review of Scientific Instruments*, **67** *(1)*, p. 55-61.
(106) Koppel, D. E. "Statistical Accuracy in Fluorescence Correlation Spectroscopy." (1974) *Phys. Rev. A*, **10**, p. 1938-1945.

(107) Qian, H. "On the Statistics of Fluorescence Correlation Spectroscopy." (1990) *Biophysical Chemistry*, **38** *(1-2)*, p. 49-57.
(108) Thompson, N. L. In *Topics in Fluorescence Spectroscopy*; Lakowicz, J. R., Ed.; Plenums Press, 1991; Vol. 1, pp 337-374.
(109) Clarke, P. A., Poele, R. T., Wooster, R. and Workman, P. "Gene expression microarray analysis in cancer biology, pharmacology, and drug development: progress and potential." (2001) *Biochemical Pharmacology*, **62** *(10)*, p. 1311-1336.
(110) Debouck, C. and Goodfellow, P. N. "DNA microarrays in drug discovery and development." (1999) *Nature Genetics*, **21**, p. 48-50.
(111) Mancinelli, L., Cronin, M. and Sadee, W. "Pharmacogenomics: The promise of personalized medicine." (2000) *Aaps Pharmsci*, **2** *(1)*, p. art. no.-4.
(112) Dyer, M. R., Cohen, D. and Herrling, P. L. "Functional genomics: from genes to new therapies." (1999) *Drug Discovery Today*, **4** *(3)*, p. 109-114.
(113) Chee, M., Yang, R., Hubbell, E., Berno, A., Huang, X. C., Stern, D., Winkler, J., Lockhart, D. J., Morris, M. S. and Fodor, S. P. A. "Accessing genetic information with high-density DNA arrays." (1996) *Science*, **274** *(5287)*, p. 610-614.
(114) Lockhart, D. J., Dong, H. L., Byrne, M. C., Follettie, M. T., Gallo, M. V., Chee, M. S., Mittmann, M., Wang, C. W., Kobayashi, M., Horton, H. and Brown, E. L. "Expression monitoring by hybridization to high-density oligonucleotide arrays." (1996) *Nature Biotechnology*, **14** *(13)*, p. 1675-1680.
(115) Duggan, D. J., Bittner, M., Chen, Y. D., Meltzer, P. and Trent, J. M. "Expression profiling using cDNA microarrays." (1999) *Nature Genetics*, **21**, p. 10-14.
(116) Heller, R. A., Schena, M., Chai, A., Shalon, D., Bedilion, T., Gilmore, J., Woolley, D. E. and Davis, R. W. "Discovery and analysis of inflammatory disease-related genes using cDNA microarrays." (1997) *Proceedings of the National Academy of Sciences of the United States of America*, **94** *(6)*, p. 2150-2155.
(117) Yuen, T., Wurmbach, E., Pfeffer, R. L., Ebersole, B. J. and Sealfon, S. C. "Accuracy and calibration of commercial oligonucleotide and custom cDNA microarrays." (2002) *Nucleic Acids Research*, **30** *(10)*, p. art. no.-e48.
(118) Kuo, W. P., Jenssen, T. K., Butte, A. J., Ohno-Machado, L. and Kohane, I. S. "Analysis of matched mRNA measurements from two different microarray technologies." (2002) *Bioinformatics*, **18** *(3)*, p. 405-412.
(119) Jenssen, T. K., Langaas, M., Kuo, W. P., Smith-Sorensen, B., Myklebost, O. and Hovig, E. "Analysis of repeatability in spotted cDNA microarrays." (2002) *Nucleic Acids Research*, **30** *(14)*, p. 3235-3244.
(120) Medh, R. D. "Microarray-based expression profiling of normal and malignant immune cells." (2002) *Endocrine Reviews*, **23** *(3)*, p. 393-400.
(121) Freeman, W. M., Walker, S. J. and Vrana, K. E. "Quantitative RT-PCR: Pitfalls and potential." (1999) *Biotechniques*, **26** *(1)*, p. 112-+.
(122) Keilholz, U., Willhauck, M., Rimoldi, D., Brasseur, F., Dummer, W., Rass, K., de Vries, T., Blaheta, J., Voit, C., Lethe, B. and Burchill, S. "Reliability of reverse transcription-polymerase chain reaction (RT-PCR)-based assays for the detection of circulating tumour cells: A quality-assurance initiative of the EORTC melanoma cooperative group." (1998) *European Journal of Cancer*, **34** *(5)*, p. 750-753.

(123) Bishop, G. A., Rokahr, K. L., Lowes, M., McGuinness, P. H., Napoli, J., DeCruz, D. J., Wong, W. Y. and McCaughan, G. W. "Quantitative reverse transcriptase-PCR amplification of cytokine mRNA in liver biopsy specimens using a non-competitive method." (1997) *Immunology and Cell Biology*, **75** *(2)*, p. 142-147.

(124) Bustin, S. A. "Quantification of mRNA using real-time reverse transcription PCR (RT-PCR): trends and problems." (2002) *Journal of Molecular Endocrinology*, **29** *(1)*, p. 23-39.

(125) Trutnau, H. H., Nölte, M., Volkmann, G., Drutchmann, D. and Blohm, D. "Genotypisierung von Hepatitis-C-Viren mittels DNA-Mikroarray-Technik dur Bioinformatik verbessert." (2003) *Biospectrum*, **9**, p. 93-95.

(126) Schwille, P., Haupts, U., Maiti, S. and Webb, W. W. "Molecular dynamics in living cells observed by fluorescence correlation spectroscopy with one- and two-photon excitation." (1999) *Biophysical Journal*, **77** *(4)*, p. 2251-2265.

(127) Bieschke, J., Giese, A., Schulz-Schaeffer, W., Zerr, I., Poser, S., Eigen, M. and Kretzschmar, H. "Ultrasensitive detection of pathological prion protein aggregates by dual-color scanning for intensely fluorescent targets." (2000) *Proceedings of the National Academy of Sciences of the United States of America*, **97** *(10)*, p. 5468-5473.

(128) Schwille, P. and Kettling, U. "Analyzing single protein molecules using optical methods." (2001) *Current Opinion in Biotechnology*, **12** *(4)*, p. 382-386.

(129) Kettling, U., Koltermann, A., Schwille, P. and Eigen, M. "Real-time enzyme kinetics monitored by dual-color fluorescence cross-correlation spectroscopy." (1998) *Proceedings of the National Academy of Sciences of the United States of America*, **95** *(4)*, p. 1416-1420.

(130) Heinze, K. G., Koltermann, A. and Schwille, P. "Simultaneous two-photon excitation of distinct labels for dual- color fluorescence crosscorrelation analysis." (2000) *Proceedings of the National Academy of Sciences of the United States of America*, **97** *(19)*, p. 10377-10382.

(131) Winkler, T., Kettling, U., Koltermann, A. and Eigen, M. "Confocal fluorescence coincidence analysis: An approach to ultra high-throughput screening." (1999) *Proceedings of the National Academy of Sciences of the United States of America*, **96** *(4)*, p. 1375-1378.

(132) Gray, N. S., Wodicka, L., Thunnissen, A.-M. W. H., Norman, T. C., Kwon, S., Espinoza, F. H., Morgan, D. O., Barnes, G., LeClerc, S., Meijer, L., Kim, S.-H., Lockhart, D. J. and Schultz, P. G. "Exploiting Chemical Libraries, Structure, and Genomics in the Search for Kinase Inhibitors." (1998) *Science*, **281**, p. 233-538.

(133) Whitecomb, D., Newton, C. R. and Little, S. "Advantages in approaches to DNA-based diagnostics." (1998) *Current Opinion in Biotechnology*, **9**, p. 602-608.

(134) Wölcke, J. and Ullmann, D. "Miniaturized HTS technologies - uHTS." (2001) *Drug Discovery Today*, **6** *(12)*, p. 637-646.

(135) Schena, M., Shalon, D., Davis, R. W. and Brown, P. O. "Quantitative Monitoring of Gene Expression Patterns with a Complementary DNA Microarray." (1995) *Science*, **270**, p. 467-470.

(136) Koltermann, A., Kettling, U., Bieschke, J., Winkler, T. and Eigen, M. "Rapid assay processing by integration of dual-color fluorescence cross-correlation spectroscopy: High throughput screening for enzyme activity." (1998)

Proceedings of the National Academy of Sciences of the United States of America, **95** *(4)*, p. 1421-1426.

(137) Mertz, J., Xu, C. and Webb, W. W. "Single-molecule detection by two-photon-excited fluorescence." (1995) *Optics Letters*, **20** *(24)*, p. 2532-2534.

(138) Barnes, M. D., Whitten, W. B. and Ramsey, J. M. "Detecting Single Molecules in Liquids." (1995) *Analytical Chemistry*, **67** *(13)*, p. A418-A423.

(139) Ambrose, W. P., Goodwin, P. M., Jett, J. H., Van Orden, A., Werner, J. H. and Keller, R. A. "Single molecule fluorescence spectroscopy at ambient temperature." (1999) *Chemical Reviews*, **99** *(10)*, p. 2929-2956.

(140) Keller, R. A., Ambrose, W. P., Arias, A. A., Gai, H., Emory, S. R., Goodwin, P. M. and Jett, J. H. "Analytical applications of single-molecule detection." (2002) *Analytical Chemistry*, **74** *(11)*, p. 316a-324a.

(141) Castro, A. and Shera, E. B. "Single-Molecule Detection - Applications to Ultrasensitive Biochemical-Analysis." (1995) *Applied Optics*, **34** *(18)*, p. 3218-3222.

(142) Rigler, R. "Fluorescence Correlations, Single-Molecule Detection and Large Number Screening - Applications in Biotechnology." (1995) *Journal of Biotechnology*, **41** *(2-3)*, p. 177-186.

(143) Mathies, R. A. and Huang, X. C. (1992) *Nature*, **359**, p. 167-169.

(144) Keller, R. A., Ambrose, W. P., Goodwin, P. M., Jett, J. H., Martin, J. C. and Wu, M. "Single molecule fluorescence analysis in solution." (1996) *Applied Spectroscopy*, **50** *(7)*, p. A12-A32.

(145) Goodwin, P. M., Cai, H., Jett, J. H., IshaugRiley, S. L., Machara, N. P., Semin, D. J., VanOrden, A. and Keller, R. A. "Application of single molecule detection to DNA sequencing." (1997) *Nucleosides & Nucleotides*, **16** *(5-6)*, p. 543-550.

(146) Demas, J. N., Wu, M., Goodwin, P. M., Affleck, R. L. and Keller, R. A. "Fluorescence detection in hydrodynamically focused sample streams: Reduction of diffusional defocusing by association of analyte with high-molecular-weight species." (1998) *Applied Spectroscopy*, **52** *(5)*, p. 755-762.

(147) Lermer, N., Barnes, M. D., Kung, C. Y., Whitten, W. B. and Ramsey, J. M. "High-Efficiency Molecular Couunting in Solution: Single-Molecule Detection in Electrodynamically Focused Microdroplet Streams." (1997) *Analytical Chemistry*, **69**, p. 2115-2121.

(148) Castro, A. and Shera, E. B. "Single-Molecule Electrophoresis." (1995) *Analytical Chemistry*, **67** *(18)*, p. 3181-3186.

(149) Fister, J. C., Jacobson, S. C., Davis, L. M. and Ramsey, J. M. "Counting single chromophore molecules for ultrasensitive analysis and separations on microchip devices." (1998) *Analytical Chemistry*, **70** *(3)*, p. 431-437.

(150) Li, Y. M., Liu, E. B. and Cheng, J. K. "Detecting single molecules in solution." (2002) *Chinese Journal of Analytical Chemistry*, **30** *(8)*, p. 1000-1004.

(151) Zander, C., Drexhage, K. H., Han, K. T., Wolfrum, J. and Sauer, M. "Single-molecule counting and identification in a microcapillary." (1998) *Chemical Physics Letters*, **286** *(5-6)*, p. 457-465.

(152) Pitschke, M., Prior, R., Haupt, M. and Riesner, D. "Detection of single amyloid beta-protein aggregates in the cerebrospinal fluid of Alzheimer's patients by fluorescence correlation spectroscopy." (1998) *Nature Medicine*, **4** *(7)*, p. 832-834.

(153) Tjernberg, L. O., Tjernberg, A., Bark, N., Shi, Y., Ruzsicska, B. P., Bu, Z. M., Thyberg, J. and Callaway, D. J. E. "Assembling amyloid fibrils from designed structures containing a significant amyloid beta-peptide fragment." (2002) *Biochemical Journal*, **366**, p. 343-351.

(154) Zhang, C., Li, W. Z. and Yun, L. H. "Application of the combinatorial chemistry to research of the natural products." (2003) *Progress in Chemistry*, **15** *(3)*, p. 194-203.

(155) Barnes, C. and Balasubramanian, S. "Recent developments in the encoding and deconvolution of combinatorial libraries." (2000) *Current Opinion in Chemical Biology*, **4** *(3)*, p. 346-350.

(156) Hsieh, F., Keshishian, H. and Muir, C. "Automated high throughput multiple target screening of molecular libraries by microfluidic MALDI-TOF MS." (1998) *Journal of Biomolecular Screening*, **3** *(3)*, p. 189-198.

(157) KieberEmmons, T., Murali, R. and Greene, M. I. "Therapeutic peptides and peptidomimetics." (1997) *Current Opinion in Biotechnology*, **8** *(4)*, p. 435-441.

(158) Carell, T., Wintner, E. A., Sutherland, A. J., Rebek, J., Dunayevskiy, Y. M. and Vouros, P. "New Promise in Combinatorial Chemistry - Synthesis, Characterization, and Screening of Small-Molecule Libraries in Solution." (1995) *Chemistry & Biology*, **2** *(3)*, p. 171-183.

(159) Clackson, T. and Wells, J. A. "In-Vitro Selection from Protein and Peptide Libraries." (1994) *Trends in Biotechnology*, **12** *(5)*, p. 173-184.

(160) Gane, P., Pecquet, C., Lambin, P., Abuaf, N., Leynadier, F. and Rouger, P. "Flow Cytometric Evaluation of Human Basophils." (1993) *Cytometry*, **14** *(3)*, p. 344-348.

(161) Stahl, S., Hansson, M., Ahlborg, N., Nguyen, T. N., Liljeqvist, S., Lundeberg, J. and Uhlen, M. "Solid-Phase Gene Assembly of Constructs Derived from the Plasmodium-Falciparum Malaria Blood-Stage Antigen Ag332." (1993) *Biotechniques*, **14** *(3)*, p. 424-&.

(162) Tang, Z. and Karnes, H. T. "Evaluation and optimization of a laboratory constructed flow chamber for on-line immunomagnetic separation." (2002) *Instrumentation Science & Technology*, **30** *(3)*, p. 295-309.

(163) Engvall, E. "Citation-Classic - Enzyme-Linked-Immunosorbent-Assay, Elisa .3. Quantitation of Specific Antibodies by Enzyme-Labeled Antiimmunoglobulin in Antigen-Coated Tubes." (1987) *Current Contents/Life Sciences (12)*, p. 16-16.

(164) Freeman, J. L., Rhyne, P. W., Dean, D. O., Beard, G. A. and Doellgast, G. J. "Isolation of antibody to human placental alkaline phosphatase (PLAP) from extracts of human placentae." (2001) *American Journal of Reproductive Immunology*, **46** *(2)*, p. 149-160.

(165) Tharakan, J. and Belizaire, M. "Ligand Efficiency in Axial and Radial Flow Immunoaffinity Chromatography of Factor-Ix." (1995) *Journal of Chromatography A*, **702** *(1-2)*, p. 191-196.

(166) Hall, R. A., Coelen, R. J. and Mackenzie, J. S. "Immunoaffinity Purification of the Ns1 Protein of Murray Valley Encephalitis-Virus - Selection of the Appropriate Ligand and Optimal Conditions for Elution." (1991) *Journal of Virological Methods*, **32** *(1)*, p. 11-20.

(167) Hawkins, R. E., Russell, S. J. and Winter, G. "Selection of Phage Antibodies by Binding-Affinity - Mimicking Affinity Maturation." (1992) *Journal of Molecular Biology*, **226** *(3)*, p. 889-896.

(168) Marks, J. D., Hoogenboom, H. R., Bonnert, T. P., McCafferty, J., Griffiths, A. D. and Winter, G. "By-Passing Immunization - Human-Antibodies from V-Gene Libraries Displayed on Phage." (1991) *Journal of Molecular Biology*, **222** *(3)*, p. 581-597.

(169) McCafferty, J., Griffiths, A. D., Winter, G. and Chiswell, D. J. "Phage Antibodies - Filamentous Phage Displaying Antibody Variable Domains." (1990) *Nature*, **348** *(6301)*, p. 552-554.

(170) Duenas, M. and Borrebaeck, C. A. K. "Clonal Selection and Amplification of Phage Displayed Antibodies by Linking Antigen Recognition and Phage Replication." (1994) *Bio-Technology*, **12** *(10)*, p. 999-1002.

(171) Krebber, C., Spada, S., Desplancq, D., Krebber, A., Ge, L. M. and Plückthun, A. "Selectively-infective phage (SIP): A mechanistic dissection of a nove in vivo selection for protein-li9gand interactions." (1997) *Journal of Molecular Biology*, **263** *(3)*, p. 607-618.

(172) Seidel, C. A. M., Schulz, A. and Sauer, M. H. M. "Nucleobase-specific quenching of fluorescent dyes. 1. Nucleobase one-electron dedox potentials and their correlation with static and dynamic quenching efficiencies." (1996) *Journal of Physical Chemistry*, **100** *(13)*, p. 5541-5553.

(173) Sanger, F., Nicklen, S. and Coulson, A. R. "DNA sequencing with chain-termination inhibitors." (1977) *Proceeding of the National Academy of Sciences of the United States of America*, **74**, p. 5463-5467.

(174) Castro, A., Fairfield, F. and Shera, B. "Detection of Single DNA-Molecules in a Sheath Flow Cuvette." (1992) *Abstracts of Papers of the American Chemical Society*, **204**, p. 51-ANYL.

(175) Goodwin, P. M., Ambrose, W. P. and Keller, R. A. "Single-molecule detection in liquids by laser-induced fluorescence." (1996) *Accounts of Chemical Research*, **29** *(12)*, p. 607-613.

(176) Dörre, K., "Machbarkeitsstudien zur DNA-Einzelmolekülsequenzierung in Mikrostrukturen" Doctoral Thesis, Technische Universität Braunschweig, Göttingen, 2000.

(177) Dörre, K., Stephan, J., Lapczyna, M., Stuke, M., Dunkel, H. and Eigen, M. "Highly efficient single molecule detection in microstructure." (2001) *Journal of Biotechnology*, **86**, p. 225-236.

(178) Ambrose, W. P., Goodwin, P. M., Martin, J. C. and Keller, R. A. "Alterations of Single-Molecule Fluorescence Lifetimes in near- Field Optical Microscopy." (1994) *Science*, **265** *(5170)*, p. 364-367.

(179) Sauer, M., Arden-Jacob, J., Drexhage, K. H., Gobel, F., Lieberwirth, U., Muhlegger, K., Muller, R., Wolfrum, J. and Zander, C. "Time-resolved identification of individual mononucleotide molecules in aqueous solution with pulsed semiconductor lasers." (1998) *Bioimaging*, **6** *(1)*, p. 14-24.

(180) Ashkin, A., Dziedzic, J. M., Bjorkholm, J. E. and Chu, S. "Observation of a Single-Beam Gradient Force Optical Trap for Dielectric Particles." (1986) *Optics Letters*, **11** *(5)*, p. 288-290.